Single-Cell Transcriptomic Profiling of the Zebrafish Inner Ear Reveals Molecularly Distinct Hair Cell and Supporting Cell Subtypes

Tuo Shi[1,2*], Marielle O. Beaulieu[3*], Lauren M. Saunders[4], Peter Fabian[1], Cole Trapnell[4], Neil Segil[1,2], J. Gage Crump[1‡], David W. Raible[3,4,5‡]

[1] Department of Stem Cell Biology and Regenerative Medicine, Keck School of Medicine, University of Southern California, Los Angeles CA 90033

[2] Caruso Department of Otolaryngology-Head and Neck Surgery, Keck School of Medicine, University of Southern California, Los Angeles CA 90033

[3] Department of Otolaryngology-Head and Neck Surgery, University of Washington, Seattle, WA 98195

[4] Department of Genomic Sciences, University of Washington, Seattle, WA 98195

[5] Department of Biological Structure, University of Washington, Seattle, WA 98195

* equal contribution

‡ Correspondence: JGC: gcrump@usc.edu

DWR: draible@uw.edu

Abstract

A major cause of human deafness and vestibular dysfunction is permanent loss of the mechanosensory hair cells of the inner ear. In non-mammalian vertebrates such as zebrafish, regeneration of missing hair cells can occur throughout life. While a comparative approach has the potential to reveal the basis of such differential regenerative ability, the degree to which the inner ears of fish and mammals share common hair cells and supporting cell types remains unresolved. Here we perform single-cell RNA sequencing of the zebrafish inner ear at embryonic through adult stages to catalog the diversity of hair cells and non-sensory supporting cells. We identify a putative progenitor population for hair cells and supporting cells, as well as distinct hair and supporting cell types in the maculae versus cristae. The hair cell and supporting cell types differ from those described for the lateral line system, a distributed mechanosensory organ in zebrafish in which most studies of hair cell regeneration have been conducted. In the maculae, we identify two subtypes of hair cells that share gene expression with mammalian striolar or extrastriolar hair cells. In situ hybridization reveals that these hair cell subtypes occupy distinct spatial domains within the three macular organs, the utricle, saccule, and lagena, consistent with the reported distinct electrophysiological properties of hair cells within these domains. These findings suggest that primitive specialization of spatially distinct striolar and extrastriolar hair cells likely arose in the last common ancestor of fish and mammals. The similarities of inner ear cell type composition between fish and mammals validate zebrafish as a relevant model for understanding inner ear-specific hair cell function and regeneration.

Introduction

Mechanosensory hair cells of the inner ear are responsible for sensing sound and head position in vertebrates. Hair cells are notoriously susceptible to damage from multiple types of insults, including noise and ototoxic drug exposure. Studies of hair cell physiology in mammals are

limited by the location of the inner ear within the temporal bone, which precludes many targeted manipulations and in vivo imaging beyond the neonatal stage. As a result, non-mammalian vertebrates with analogous, more easily accessible hair cells have become useful models for studying hair cell development, death, and regeneration. Non-mammalian vertebrates such as birds and fish can regenerate hair cells of the auditory and vestibular systems that are lost due to injury (Stone and Cotanche, 2007; Monroe et al., 2015). This differs from mammals, where cochlear hair cell death leads to permanent hearing loss (Corwin and Cotanche, 1988; Yamasoba and Kondo, 2006), and limited regeneration of vestibular hair cells results in minimal recovery of function (Golub et al., 2012). Non-mammalian model systems of hair cell regeneration have the potential to reveal conserved pathways that can be targeted to promote hair cell survival and regeneration in humans. However, the extent of hair cell molecular homology across vertebrates remains unclear.

Due to its accessibility for manipulation and imaging, the zebrafish lateral line system has been widely used to study mechanisms of hair cell physiology (Pickett and Raible, 2019; Sheets et al., 2021). The lateral line is an external sensory system that allows aquatic vertebrates to detect local movement of water. Sensory organs of the lateral line, called neuromasts, contain hair cells and supporting cells that share properties with those of the inner ear. However, relative to the lateral line, cells in the zebrafish inner ear are likely more similar to their mammalian counterparts, raising the potential for it to be a more comparable system in which to study hair cell function.

Zebrafish and mammals share several inner ear sensory organs. Three semicircular canals with sensory end organs called cristae sense angular rotation of the head. Two additional sensory end organs detect linear acceleration and gravity: the utricular and saccular macula each with an associated otolith crystal (Figure 1). Fish lack a specific auditory structure such as the

70 mammalian cochlea and instead sense sound through the saccule, utricle, and a third otolith
71 organ, the lagena. Although historically the saccule and utricle were thought to be for vestibular
72 function and the lagena analogous to the cochlea for sound detection, there is now substantial
73 evidence for all three otolith end organs being used for sound detection with diverse
74 specializations across fishes (Popper and Fay, 1993). Zebrafish exhibit behavioral responses to
75 sound frequencies between 100-1200 Hz (Zeddies and Fay, 2005; Bhandiwad et al., 2013), and
76 neural responses up to 4000 Hz (Poulsen et al., 2021). In larval zebrafish, both saccule and
77 utricle hair cells respond to vibration stimuli, with the utricle responding to relatively lower
78 frequencies than the saccule, as well as additive effects when both are stimulated (Yao et al.,
79 2016, Favre-Bulle et al., 2020).
80
81 Within the mammalian utricle and saccule, there are both morphological and spatial differences
82 between hair cells (Lysakowski and Goldberg, 2004; Eatock and Songer, 2011). Hair cells are
83 broadly classified by their morphology and innervation, with Type I hair cells having calyx
84 synapses surrounding the hair cell body and Type II hair cells having bouton synapses. Both
85 Type I and Type II cells can be found within the central region of the macular organs known as
86 the striola and in the surrounding extrastriolar zones. Although the role of spatial segregation
87 into striolar versus extrastriolar zones has not been fully elucidated, hair cells across these
88 regions vary in morphology, electrophysiology, and synaptic structure (Desai et al., 2005; Li et
89 al., 2008). The striola is characterized by hair cells with taller ciliary bundles and encompasses
90 a line of polarity reversal where hair cells change their stereocilia orientation (Figure 1E).
91 Whereas distinct Type I and Type II hair cells, and in particular the calyx synapses typical of
92 Type I cells, have not been identified in fishes, spatial heterogeneity in the maculae, including
93 those of zebrafish, has been previously noted (Chang et al., 1992; Platt, 1993; Popper, 2000;
94 Liu et al., 2022). However, the homologies of cells at the cellular and molecular levels have
95 remained unknown.

96

97 Recent single-cell and single-nucleus RNA-sequencing efforts have generated a wealth of
98 transcriptomic data from hair cells in several model systems, facilitating more direct comparison
99 of cell types and gene regulatory networks between species. Although single-cell transcriptomic
100 data have recently been published for the zebrafish inner ear (Jimenez et al., 2022; Qian et al.,
101 2022), the diversity of hair cell and supporting cell subtypes has not been thoroughly analyzed.
102 In order to better understand the diversification of cell types in the zebrafish inner ear, and their
103 relationships to those in mammals, here we perform single-cell and single-nucleus RNA
104 sequencing of the zebrafish inner ear from embryonic through adult stages. We find that hair
105 and supporting cells from the zebrafish inner ear and lateral line are transcriptionally distinct,
106 and that hair and supporting cells differ between the cristae and maculae. All of these distinct
107 cell types are present during larval development and are maintained into adulthood. In situ
108 hybridization reveals that these hair cell subtypes occupy distinct spatial domains within the
109 utricle, saccule, and lagena, and computational comparison of hair cell types reveals homology
110 with striolar and extrastriolar hair cell types in mammals. These findings point to an origin of
111 striolar and extrastriolar hair cell types in at least the last common ancestor of fish and
112 mammals.

113

114 **Results**

115 **Inner ear hair cells and supporting cells are distinct from those of the lateral line**

116 To assess differences between inner ear and lateral line cells, we analyzed a subset of cells
117 from a large single-nucleus RNA-seq dataset of whole zebrafish at embryonic and larval stages
118 (24-96 hours post-fertilization (hpf)), which was prepared by single-nucleus combinatorial
119 indexing and sequencing ("sci-Seq"; Saunders et al., 2022). Within an initial dataset of 1.25
120 million cells from 1233 embryos spanning 18 timepoints between 18 and 96 hours (see
121 Saunders et al., 2022 for more detail), a total of 16,517 inner ear and lateral line cells were

isolated, combined, and re-processed using Monocle 3 (Figure 2A-B). Initially, otic vesicle and lateral line cell clusters were identified by *eya1* expression (Sahly et al., 1999) in combination with the following known marker genes. Inner ear nonsensory cells were identified by expression of the transcription factor gene *sox10* (Dutton et al., 2009) in combination with inner ear supporting cell genes *(stm*, *otog*, *otogl*, *otomp*, *tecta*, and *oc90*; Figure 2C) (Söllner et al., 2003; Kalka et al., 2019; Petko et al., 2008; Stooke-Vaughan et al., 2015). Lateral line nonsensory cells were identified by expression of known markers *fat1b*, *tfap2a, tnfsf10l3, lef1, cxcr4b, fgfr1a*, and *hmx3a* (Figure 2D) (Steiner et al., 2014; Thomas and Raible, 2019; McGraw et al., 2011; Haas and Gilmour, 2006; Lee et al., 2016; Feng and Xu, 2010). We identified hair cells by expression of the pan-hair cell genes *otofb*, *cdh23, pcdh15a, ush1c, myo7aa, slc17a8*, and *cacna1da* (Figure 2E) (Chatterjee et al., 2015; Söllner et al., 2004; Seiler et al., 2005; Phillips et al., 2011; Ernest et al., 2000; Obholzer et al., 2008; Sheets et al., 2012). To distinguish between inner ear and lateral line hair cells, we queried expression of previously described markers for inner ear (*gpx2*, *kifl*, *strc*, and *lhfpl5a*) and lateral line (*strc1*, *lhfpl5b*, and *s100t*) (Erickson et al., 2019; Erickson and Nicolson, 2015). Although many of these markers are at low abundance, these populations are marked distinctly by *strc* and *s100t* (Figure 2F). We used Monocle3 to identify differentially expressed genes (Supplementary File 1) and to generate modules of co-expressed genes (Figure 2-figure supplement 1, Supplementary File 2).

Both hair cells and nonsensory supporting cells from the inner ear and lateral line formed distinct clusters, with nonsensory cells from the two mechanosensory organs showing greater distinction than hair cells (Figure 2B, Figure 2-figure supplement 2A). To confirm the relative differences between inner ear and lateral line hair cells and nonsensory cells, Partition-based Graph Abstraction (PAGA) analysis was used to measure the connectivity of clusters (Wolf et al., 2019). PAGA analysis revealed strong connectivity within inner ear supporting cell clusters

and within lateral line supporting cell clusters but little connectivity between them (Figure 2-figure supplement 2A, Supplementary File 3).

The inner ear nonsensory cluster includes structural cells forming the otic capsule, identified by expression of the extracellular matrix protein-encoding genes *collagen type 2 a1a* (*col2a1a*) and *matrilin 4* (*matn4*) (Xu et al., 2018), as well as sensory supporting cells expressing *lfng* (Figure 3D; Figure 2-figure supplement 2B). Inner ear and lateral line supporting cells remain as distinct clusters even when structural *matn4*+ cells are excluded from analysis (Figure 2-figure supplement 2C). Thus, both hair cells and supporting cells have distinct gene expression profiles between the inner ear and lateral line at embryonic and larval stages.

Single-cell RNA-seq reveals distinct hair cell and supporting cell populations in the juvenile and adult inner ear of zebrafish

To identify distinct subtypes of inner ear hair cells and supporting cells from larval through adult stages, we first re-analyzed single-cell RNA sequencing (scRNA-seq) datasets from larval stages (72 and 120 hpf) (Fabian et al., 2022), in which otic placode cells and their descendants were labeled with *Sox10*:Cre to induce recombination of an ubiquitous *ubb*:LOXP-EGFP-STOP-LOXP-mCherry transgene (Kague et al., 2012). We also performed additional scRNA-seq using these transgenic lines by dissecting ears from juvenile (14 days post-fertilization (dpf)), and adult (12 months post-fertilization (mpf)) animals. Following cell dissociation and fluorescence-activated cell sorting (FACS) to purify mCherry+ cells, we constructed scRNA-seq libraries using 10x Chromium technology. For all datasets, hair cells and supporting cells were identified for further analysis based on the expression of hair cell markers *myo6b* and *strc* and supporting cell markers *stm* and *lfng*; structural cells were removed from further analysis based on expression of *matn4* and *col2a1a* (Figure 3-figure supplement 1). Using Seurat, we integrated this dataset with the sci-Seq embryonic and larval dataset (36-96 hpf) (Figure 3A,B). The combined dataset

comprises 3246 inner ear cells separated into 10 groups based on unsupervised clustering, with differentially expressed genes for each cluster shown in Figure 3E and Supplementary File 4. We identified 6 clusters of hair cells based on shared expression of *myo6b*, *strc*, *lhfpl5a*, and *gfi1aa* (Yu et al., 2020), a nascent hair cell cluster based on expression of *atoh1a* (Millimaki et al., 2007) and the Notch ligand *dla* (Riley et al., 1999), and two clusters of supporting cells based on expression of *lfng* and *stm* (Figure 3C,D, Figure 3-figure supplement 2). An additional putative progenitor cluster (cluster 0), enriched for cells from embryonic stages, is characterized by expression of genes such as *fgfr2* (Rohs et al., 2013), *fat1a* (Down et al, 2005), *igsf3*, and *pard3bb* (Figure 3-figure supplement 3). Although these marker genes are differentially expressed in the putative progenitor cluster, some of them (e.g. *fat1a* and *pard3bb*) retain a lower expression level in supporting cell populations (Figure 3-figure supplement 3F). This is further demonstrated by gene modules of these clusters (Figure 3-figure supplement 4, Supplementary File 5), where the progenitor signature module genes (Module 1) are expressed in lower levels in the supporting cell clusters. This transcriptional relatedness between progenitors and supporting cells may underlie the role of supporting cells as a resident stem cell population during zebrafish hair cell regeneration.

Developmental trajectories in the inner ear

To understand potential lineage relationships between clusters, we performed pseudotime trajectory analysis using Monocle3. We anchored the pseudotime projection at the putative progenitor cell cluster. Analysis revealed two major trajectories toward hair cells and supporting cell clusters for both maculae and cristae (Figure 4A,B, Figure 4-figure supplement 1), with distinct patterns of gene expression along each trajectory (Supplementary File 6). We find that average gene expression of the putative progenitor (Cluster 0) markers follow two patterns: decreasing along both hair cell and supporting cell trajectories (*fgfr2* and *igsf3*) and decreasing only along the hair cell trajectory (*fat1a* and *pard3bb*) (Figure 4C,D, Figure 4-figure supplement

1B,C). The hair cell trajectory progresses first through a stage marked by expression of *dla* and then *atoh1a* (Cluster 2, Figure 4E, Figure 4-figure supplement 1D). Concurrent with decreasing expression of nascent hair cell genes, we observe increasing expression of mature hair cell genes *gfi1aa* and *myo6b* (Figure 4F, Figure 4-figure supplement 1E). Along the supporting cell trajectory we observed upregulation of supporting cell-specific markers, including *stm* and *lfng* (Figure 4G, Figure 4-figure supplement 1F). These bifurcating lineage trajectories from Cluster 0 (Figure 4A) to hair and supporting cell clusters are consistent with the identification of Cluster 0 as a population of bipotent progenitors regulated by Notch signaling during early development (Haddon et al., 1998; Riley et al., 1999). To localize these developmental stages in vivo, we examined *dla* expression by in situ hybridization (Figure 4-figure supplement 2). We find that *dla* is expressed in supporting cells adjacent to myo6:GFP hair cells in both cristae and maculae, consistent with peripheral addition of new cells at the margins of the sensory patches.

Distinct supporting cell types in the cristae versus maculae

Supporting cells comprise two major clusters that can be distinguished by expression of *tectb* and *zpld1a* among other genes (Figure 3C, see Supplementary File 7 for differentially expressed genes). The *tectb* gene encodes Tectorin beta, a component of the tectorial membrane associated with cochlear hair cells in mammals (Goodyear et al., 2017), and a component of otoliths in zebrafish (Kalka et al., 2019). The z*pld1a* gene, encoding Zona-pellucida-like domain containing protein 1a, is expressed in the cristae in fish (Dernedde et al., 2014; Yang et al., 2011) and mouse (Vijayakumar et al., 2019). Using fluorescent in situ hybridization, we find that *tectb* is expressed in the macular organs but not cristae, and *zpld1a* is expressed in cristae but not maculae (Figure 5C,D). Neither were detected in lateral line neuromasts (Figure 5C,D), showing they are inner ear-specific genes. Both *tectb* and *zpld1a* are expressed primarily in supporting cells, as they show little overlap in expression with the hair cell marker *myo6b*:GFP, similar to expression of the supporting cell marker *lfng* (Figure 5B-D,

Figure 5-figure supplement 1). These results demonstrate the presence of distinct supporting cell subtypes for the maculae and cristae.

Distinct types of hair cells in the zebrafish inner ear

While inner ear and lateral line hair cells share many structural and functional features, we sought to determine if these cells also have distinct molecular signatures. We compared published datasets of lateral line hair cells (Baek et al., 2022; Kozak et al., 2020; Ohta et al., 2020) to our data, restricting analysis to datasets generated by 10x Chromium preparation to avoid technical batch effects across studies. Using Scanorama for alignments (Hie et al., 2019), hair cells from the inner ear and lateral line form distinct clusters, with a number of differentially expressed genes (Figure 2-figure supplement 3), including the known markers for lateral line (*s100t*) and inner ear (*strc*) (Figure 2). This analysis suggests that inner ear hair cells of the maculae and cristae are more similar to each other than to lateral line hair cells.

Within the maculae and cristae, we find that hair cells can be subdivided into two major groups (clusters 1 and 3 versus cluster 4). These clusters are distinguished by differential expression of a number of genes including two calcium binding protein genes, *cabp1b* and *cabp2b* (Di Donato et al., 2013) (Figure 3E). Hair cell cluster 5 has a mixed identity with co-expression of a number of genes shared between these two groups, including *cabp1b* and *cabp2b*.

We next tested the in vivo expression of genes in each cluster using in situ hybridization, choosing *cabp1b* and *cabp2b* as representative markers for each cluster (Figure 6A). In the larval cristae, utricle, and saccule, *cabp1b* and *cabp2b* mark *myo6b*+ hair cells in largely non-overlapping zones (Figure 6B-D). By adult stages, complementary domains of *cabp1b*+ and *cabp2b*+ hair cells become clearly apparent (Figure 6E-K). In the adult utricle, a central crescent of *cabp2b*+*; myo6b*+ hair cells is surrounded by a broad domain of *cabp1b*+; *myo6b*+ hair cells.

In the saccule and lagena, a late developing sensory organ, central *cabp2b+; myo6b+* hair cells are surrounded by peripheral *cabp1b+; myo6b+* hair cells. We also find several genes that are specific for hair cells in the cristae, utricle, or saccule (Figure 7A). These include the calcium binding protein gene *cabp5b* in the cristae, the transcription factor *skor2* in the utricle, and the deafness gene *loxhd1b* in the saccule (Figure 7B-D, Figure 7-figure supplement 1).

The domain organization of hair cells in the adult macular organs resembles that of striolar and extrastriolar hair cells in the mammalian utricle. We therefore examined expression of *pvalb9*, the zebrafish ortholog of the mouse striolar hair cell marker *Ocm* (Hoffman et al., 2018; Jiang et al., 2017) (Figure 8, Figure 8-figure supplement 1). In the larval utricle, we observe near complete overlap of *pvalb9* with *cabp2b* (Figure 8B-D). In the adult utricle, there is substantial overlap of *pvalb9* with *cabp2b* expression (except for a thin strip of *pvalb9+*; *cabp2b-* cells), and little overlap with *cabp1b* expression (Figure 8F,G). In addition, anti-Spectrin staining of hair bundles reveals a line of polarity reversal within the *cabp2b+* domain of the utricle (Figure 8H,I), consistent with polarity reversal occurring within the striolar domains of mammalian macular organs (Li et al., 2008). Cluster 1/3 (*cabp1b+*) and Cluster 4 (*cabp2b+*) populations also differentially express genes related to stereocilia tip link and mechanotransduction channel components (Figure 8-figure supplement 2, Supplementary File 8) and various calcium and potassium channels (Figure 8-figure supplement 3, Supplementary File 8). We also note that the utricle marker *skor2* labels primarily extrastriolar hair cells within this end organ, with *loxhd1b* labeling striolar hair cells within the saccule. These findings suggest that zebrafish Cluster 4 (*cabp2b+*) and Cluster 1/3 (*cabp1b+*) hair cells largely correspond to striolar and extrastriolar hair cells, respectively, with distinct mechanotransduction and synaptic properties.

Global homology of striolar and extrastriolar hair cells between fish and mice

To further probe similarities between zebrafish Cluster 4 (*cabp2b*+) and Cluster 1/3 (*cabp1b*+) hair cells versus striolar and extrastriolar hair cells in mammals, we utilized the Self-Assembling Manifold mapping (SAMap) algorithm (Tarashansky et al., 2021; Musser et al., 2021) to compare cell types across distant species. A strength of this algorithm is that it compares not only homologous gene pairs but also close paralogs, which is especially useful considering the extensive paralog switching observed between vertebrate clades (Postlethwait, 2007), as well as the extra round of genome duplication in the teleost lineage leading to zebrafish. When comparing adult zebrafish maculae with the postnatal mouse utricle (Jan et al., 2021), we find the highest alignment score between supporting cells (Figure 9A). Consistent with the spatial domains revealed by our in situ gene expression analysis, we find that mouse striolar Type I hair cells exclusively map to zebrafish Cluster 4 (*cabp2b*+) hair cells, and mouse extrastriolar Type I and Type II hair cells predominantly to zebrafish Cluster 1/3 (*cabp1b*+) hair cells. In contrast, zebrafish lateral line hair cells (Lush et al., 2019) align exclusively to mouse extrastriolar and not striolar hair cells (Figure 9-figure supplement 1). The small degree of mapping of mouse extrastriolar Type I hair cells to zebrafish Cluster 4 (*cabp2b*+) hair cells suggests that zebrafish Cluster 4 (*cabp2b*+) hair cells may have more of a Type I identity than Cluster 1/3 (*cabp1b*+) cells in general. Gene pairs driving the homology alignment include striolar markers *Ocm*, *Loxhd1*, and *Atp2b2* for zebrafish Cluster 4 (*cabp2b*+) hair cells, and mouse extrastriolar markers *Tmc1*, *Atoh1*, and *Jag2* for zebrafish Cluster 1/3 (*cabp1b*+) hair cells (Supplementary File 9). Thus, zebrafish Cluster 4 (*cabp2b*+) macular hair cells are closely related to striolar cells of the mouse utricle, with zebrafish lateral line and Cluster 1/3 (*cabp1b*+) macular hair cells more closely related to mouse extrastriolar hair cells.

A recent single-cell study revealed distinct central versus peripheral hair cell subpopulations in postnatal mouse cristae, reminiscent of the striolar and extrastriolar populations in the maculae (Wilkerson et al., 2021). As our zebrafish cristae hair cells also separate into distinct clusters,

Cluster 9 (*cabp1b*+) and Cluster 8 (*cabp2b*+) (Figure 6A,B), we performed SAMap analysis between the crista cell populations of the two species to investigate cell type homology. Similar to what we observed for the utricle, zebrafish centrally located Cluster 8 crista hair cells predominantly map to mouse central crista hair cells, and zebrafish peripherally located Cluster 9 crista hair cells exclusively map to mouse peripheral crista hair cells (Figure 9B, see Supplementary Files 10 and 11 for differentially expressed genes in Cluster 8 and Cluster 9 hair cells and gene pairs driving homology). Conserved types of spatially segregated HCs therefore exist in both the maculae and cristae of zebrafish and mouse.

Discussion

Our single-cell transcriptomic profiling of the embryonic to adult zebrafish inner ear reveals a diversity of hair cell and supporting cell subtypes that differ from those of the lateral line. As much of our knowledge about zebrafish hair cell regeneration comes from studies of the lateral line, understanding similarities and differences between the lateral line and inner ear has the potential to uncover mechanisms underlying the distinct regenerative capacity of inner ear hair cell subtypes. Recent tools to systematically damage inner ear hair cells in zebrafish (Jimenez et al., 2021) should enable such types of comparative studies.

We identify hair cells and supporting cells specific for maculae versus cristae, as well as two spatially segregated types of zebrafish inner ear hair cells with similarities to mammalian striolar and extrastriolar hair cells. These molecular signatures are conserved across larval and adult stages. However, consistent with other recent work (Jimenez et al., 2022, Qian et al., 2022), we were not able to resolve distinct clusters of hair cells or supporting cells corresponding to the distinct types of maculae: i.e. utricle, saccule, and lagena.

327 The division of auditory and vestibular function across the otolith organs in zebrafish remains
328 somewhat unclear. The saccule is thought to act as the primary auditory organ of larval
329 zebrafish, as the utricle is not necessary for sound detection above low frequencies (Yao et al.,
330 2016). In the zebrafish adult, excess sound exposure can damage the saccule, while damage to
331 the utricle is unknown (Schuck and Smith, 2009). Conversely, the utricle is critical for larval
332 vestibular function, while input from the saccule is unnecessary (Riley and Moorman, 2000).
333 However, there is contrasting evidence for overlap in function of both saccule and utricle for
334 sound detection in larvae (Favre-Bulle et al 2020; Poulsen et al. 2021). Currently we are not
335 able to identify clearly distinct hair cell types in the utricle compared to the saccule that might
336 reflect functional differences; whether such genetic signatures exist remains an important
337 question that will require further in-depth analysis. It is interesting to note that mammalian
338 vestibular end organs are also capable of responding to high-frequency sound stimuli (reviewed
339 in Curthoys, 2017), suggesting that sound detection by hair cells may not be linked to a distinct
340 end organ-specific molecular signature.
341
342 Our study supports zebrafish possessing distinct types of striolar and extrastriolar hair cells in
343 the maculae and cristae, with molecular differences between these subtypes implying different
344 physiological properties. Zebrafish striolar and extrastriolar hair cell subtypes express distinct
345 combinations of ion channel genes and mechanotransduction components, consistent with
346 previous reports of distinct current profiles in central versus peripheral hair cells in the zebrafish
347 utricle, saccule, and lagena (Haden et al., 2013; Olt et al., 2014), as well as spatial differences
348 in ciliary bundle morphology and synaptic innervation in the larval zebrafish utricle (Liu et al.,
349 2022). The distinct spatial distribution, channel expression, and hair bundle morphologies in
350 these hair cells resembles the known spatial, electrophysiological, and hair bundle
351 compositional differences seen in the striolar versus extrastriolar hair cells in the amniote

vestibular end organs (Holt et al., 2007; Kharkovets et al., 2000; Lapeyre et al., 1992; Meredith and Rennie, 2016; Moravec and Peterson, 2004; Rüsch et al., 1998; Xue and Peterson, 2006).

In each of the zebrafish end organs, striolar and extrastriolar hair cells can be defined by differential expression of calcium binding proteins, in particular *cabp1b* versus *cabp2b*. As these calcium binding proteins closely interact with synaptic calcium channels (Cui et al., 2007; Pitcher et al., 2017) with potential functionally different consequences (Yang et al., 2018), their differential expression may confer unique electrophysiological properties to each cell type. Mutations in human *CABP2* associated with the autosomal recessive locus DFNB93 result in hearing loss (Schrauwen, et al., 2012; Pitcher et al., 2017), underlining its functional importance. Even though we chose *cabp1b* and *cabp2b* as characteristic markers for zebrafish extrastriolar and striolar regions, it is worth noting that *Cabp2*, but not *Cabp1*, is expressed in all mouse postnatal utricular hair cells with differentially higher expression in the striola (Jan et al., 2021). Of note, lateral line hair cells express higher levels of *cabp2b* than *cabp1b* (Lush et al., 2019), despite our analysis suggesting that they are more closely related to extrastriolar hair cells. These observations emphasize the importance of examining global patterns of gene expression rather than individual markers when assigning homology of cell types.

By contrast, we found no clear homology of zebrafish inner ear hair cells with mammalian Type I and Type II hair cells. The lack of molecular signatures corresponding to Type I hair cells is consistent with previous reports that one of their major features, calyx synapses, are absent from fishes (Lysakowski and Goldberg, 2004). These findings suggest that the diversification of inner ear hair cells into Type I and Type II cells emerged after the evolutionary split of ray-finned fishes from the lineage leading to mammals.

377 We recognize that identifying cell type homology across tissues and species through molecular
378 analysis has several potential caveats. Although we have collected transcriptomic data from the
379 zebrafish inner ear from a wide range of developmental stages, we are limited by the fact that
380 the publicly available datasets for zebrafish lateral line and mouse utricle and cristae are
381 restricted to immature stages. Thus, cell maturity could be a confounder in our analyses.
382 However, when we limited the comparison of lateral line hair cells and postnatal mouse
383 vestibular hair cells to 3-5 dpf inner ear hair cells, we see similar alignments as when we used
384 our 12 mpf data (Figure 9-figure supplement 1). In addition, we collected fewer supporting cells
385 from adult zebrafish than expected, skewing cell type representation towards hair cells (Figure
386 3C). Thus, additional optimization may be needed to further interrogate the cell subtypes within
387 zebrafish inner ear supporting cell populations.
388
389 Nonetheless, our integrated dataset reveals distinct molecular characteristics of hair cells and
390 supporting cells in the zebrafish inner ear sensory organs, with conservation of these patterns
391 from larval stages to adults. Although not discussed in detail here, our data include additional
392 cell populations of the zebrafish inner ear that express extracellular matrix-associated genes
393 important for otic capsule structure and ion channel-associated genes associated with fluid
394 regulation. These data form a resource that can be further explored to inform molecular aspects
395 of hair cell electrophysiology, mechanotransduction, sound versus motion detection,
396 maintenance of inner ear structure and ionic balance, and inner ear-specific hair cell
397 regeneration.
398
399 **Materials and Methods**
400 **Zebrafish lines**
401 This study was performed in strict accordance with the recommendations in the Guide for the
402 Care and Use of Laboratory Animals of the National Institutes of Health. The Institutional Animal

Care and Use Committees of the University of Southern California (Protocol 20771) and University of Washington (Protocol 2997-01) approved all animal experiments. Experiments were performed on zebrafish (*Danio rerio*) of AB or mixed AB/Tubingen background. For adult stages, mixed sexes of animals were used for constructing single-cell libraries, as well as RNAScope experiments. Published lines include *Tg(Mmu.Sox10-Mmu.Fos:Cre)*^{zf384} (Kague et al., 2012); *Tg(-3.5ubb:LOXP-EGFP-STOP-LOXP-mCherry)*^{cz1701Tg} (Mosimann et al., 2011); and *Tg(myosin 6b:GFP)*^{w186} (Hailey et al., 2017).

In situ hybridization and RNAScope

Hybridization chain reaction in situ hybridizations (Molecular Instruments, HCR v3.0) were performed on 5 dpf *myo6b*:GFP larvae as directed for whole-mount zebrafish embryos and larvae (Choi et al., 2016, 2018). Briefly, embryos were treated with 1-phenyl 2-thiourea (PTU) beginning at 24 hpf. At 5 dpf, larvae were fixed in 4% PFA overnight at 4°C. Larvae were washed with PBS and then stored in MeOH at -20°C until use. Larvae were rehydrated using a gradation of MeOH and PBST washes, treated with proteinase K for 25 min and post-fixed with 4% PFA for 20 min at room temperature. For the detection phase, larvae were pre-hybridized with a probe hybridization buffer for 30 min at 37°C, then incubated with probes overnight at 37°C. Larvae were washed with 5X SSCT to remove excess probes. For the amplification stage, larvae were pre-incubated with an amplification buffer for 30 min at rt and incubated with hairpins overnight in the dark at rt. Excess hair pins were removed by washing with 5X SSCT. Larvae were treated with DAPI and stored at 4°C until imaging. All HCR in situ patterns were confirmed in at least 3 independent animals. Transcript sequences submitted to Molecular Instruments for probe generation are listed in Supplementary File 12. The *cabp1b* probes were tested on 3 separate occasions and imaged in at least 6 animals; *cabp2b* probes were tested on 5 separate occasions and imaged in at least 20 different animals; *cabp5b* probes were tested on 3 separate occasions and imaged in at least 9 different animals; *lfng* probes were tested on two

separate occasions and imaged in at least 5 different animals; *loxhd1b* probes were tested on two separate occasions and imaged in at least 7 animals; *pvalb9* probes were tested on two separate occasions and imaged in at least 6 different animals; *skor2* probes were tested on two separate occasions and imaged in at least 6 different animals; *tectb* probes were tested on 4 separate occasions and imaged in at least 10 different animals; *zpld1a* probes were tested on 3 separate occasions and imaged in at least 9 different animals.

RNAScope samples were prepared by fixation in 4% paraformaldehyde either at room temperature for 2 hours or at 4 °C overnight. Adult (28-33mm) inner ears were dissected and dehydrated in methanol for storage. RNAScope probes were synthesized by Advanced Cell Diagnostics (ACD): Channel 1 probe *myo6b* (1045111-C1), Channel 2 probe *pvalb9* (1174621-C2), and Channel 3 probes *cabp1b* (1137731-C3) and *cabp2b* (1137741-C3). Whole inner ear tissues were processed through the RNAScope Fluorescent Multiplex V2 Assay (ACD Cat. No. 323100) according to manufacturer's protocols with the ACD HybEZ Hybridization oven. *cabp1b* probe was tested on 4 separate occasions with 6 animals or 12 ears total; *cabp2b* probe was tested on 4 separate occasions with 7 animals or 14 ears total; *pvalb9* probe was tested on 2 separate occasions with 6 animals or 12 ears total. *myo6b* probe was used with each of the above probes.

Immunofluorescence staining

Immediately following the RNAScope protocol, samples were prepared for immunofluorescence staining using mouse anti-β-Spectrin II antibody (BD Bioscience Cat. No. 612562, RRID: AB_399853). Briefly, RNAScope probed zebrafish ears were rehydrated in PBS for 5 min and rinsed in PBDTx (0.5 g bovine serum albumin, 500 µL DMSO, 250 µL 20% Triton-X in 50 mL PBS, pH = 7.4) for 15 min at room temperature. They were then blocked in 2% normal goat serum (NGS) in PBDTx for 3 hours at room temperature, and incubated with 1:500 dilution of

mouse anti-β-Spectrin II antibody in PBDTx containing 2% NGS overnight at 4 °C. After 3 washes in PBDTx for 20 min each at room temperature, samples were incubated with 1:1000 dilution of Alexa 647 goat-anti-mouse IgG1 secondary antibody (Invitrogen Cat. No. A-21240, RRID: AB_2535809) for 5 hours at room temperature. They were then washed 2 times in PBSTx (250 µL 20% Triton-X in 50 mL PBS) for 5 min each before imaging. Three animals or 6 ears total were subjected to Spectrin detection on 2 separate occasions.

Imaging

Confocal images of whole-mount RNAScope samples were captured on a Zeiss LSM800 microscope (Zeiss, Oberkochen, Germany) using ZEN software. HCR-FISH imaging was performed on a Zeiss LSM880 microscope (Zeiss, Oberkochen, Germany) with Airyscan capability. Whole larvae were mounted between coverslips sealed with high vacuum silicone grease (Dow Corning) to prevent evaporation. Z-stacks were taken through the ear at intervals of 1.23 µm using a 10X objective or through individual inner ear organs at an interval of 0.32 µm using a 20X objective. 3D Airyscan processing was performed at standard strength settings using Zen Blue software.

Single-cell preparation and analysis

scRNA-seq library preparation and alignment

For 14 dpf animals (n=35), heads from converted *Sox10:Cre; ubb:LOXP-EGFP-STOP-LOXP-mCherry* fish were decapitated at the level of the pectoral fin with eyes and brains removed. For 12 mpf animals (n=6, 27-31mm), utricle, saccule, and lagena were extracted from converted *Sox10:Cre; ubb:LOXP-EGFP-STOP-LOXP-mCherry* fish after brains and otolith crystals were removed. Dissected heads and otic sensory patches were then incubated in fresh Ringer's solution for 5–10 min, followed by mechanical and enzymatic dissociation by pipetting every 5 min in protease solution (0.25% trypsin (Life Technologies, 15090-046), 1 mM EDTA, and

400 mg/mL Collagenase D (Sigma, 11088882001) in PBS) and incubated at 28.5 °C for 20–30 min or until full dissociation. Reaction was stopped by adding 6× stop solution (6 mM CaCl2 and 30% fetal bovine serum (FBS) in PBS). Cells were pelleted (376 × g, 5 min, 4 °C) and resuspended in suspension media (1% FBS, 0.8 mM CaCl2, 50 U/mL penicillin, and 0.05 mg/mL streptomycin (Sigma-Aldrich, St. Louis, MO) in phenol red-free Leibovitz's L15 medium (Life Technologies)) twice. Final volumes of 500 µL resuspended cells were placed on ice and fluorescence-activated cell sorted (FACS) to isolate live cells that excluded the nuclear stain DAPI. For scRNAseq library construction, barcoded single-cell cDNA libraries were synthesized using 10X Genomics Chromium Single Cell 3′ Library and Gel Bead Kit v.3.1 (14 dpf) or Single Cell Multiome ATAC + Gene Expression kit (12 mpf, single library built with all three sensory patches combined prior to library preparation, ATAC data not shown) per the manufacturer's instructions. Libraries were sequenced on Illumina NextSeq or HiSeq machines at a depth of at least 1,000,000 reads per cell for each library. Read2 was extended from 98 cycles, per the manufacturer's instructions, to 126 cycles for higher coverage. Cellranger v6.0.0 (10X Genomics) was used for alignment against GRCz11 (built with GRCz11.fa and GRCz11.104.gtf) and gene-by-cell count matrices were generated with default parameters.

Data processing of scRNA-seq

Count matrices of inner ear and lateral line cells from embryonic and larval timepoints (18-96 hpf) were analyzed using the R package Monocle3 (v1.0.0) (Cao et al., 2019). Matrices were processed using the standard Monocle3 workflow (preprocess_cds, detect_genes, estimate_size_factors, reduce_dimension(umap.min_dist = 0.2, umap.n_neighbors = 25L)). This cell data set was converted to a Seurat object for integration with 10X Chromium sequencing data using SeuratWrappers. The count matrices of scRNA-seq data (14 dpf and 12 mpf) were analyzed by R package Seurat (v4.1.0) (Hao et al., 2021). Cells of neural crest origins were removed bioinformatically based on our previous study (Fabian et al., 2022). The matrices were

normalized (NormalizeData) and integrated with normalized scRNA-seq data from the embryonic and larval time points according to package instruction (FindVariableFeatures, SelectIntegrationFeatures, FindIntegrationAnchors, IntegrateData; features = 3000). The integrated matrices were then scaled (ScaleData) and dimensionally reduced to 30 principal components. The data were then subjected to neighbor finding (FindNeighbors, k = 20) and clustering (FindClusters, resolution = 0.5), and then visualized through UMAP with 30 principal components as input. After data integration and processing, RNA raw counts from all matrices were normalized and scaled according to package instructions to determine gene expression for all sequenced genes, as the integrated dataset only contained selected features for data integration.

Mouse utricle scRNA-seq data (Jan et al., 2021) was downloaded from NCBI Gene Expression Omnibus (GSE155966). The count matrix was analyzed by R package Seurat (v4.1.0). Matrices were normalized (NormalizeData) and scaled for the top 2000 variable genes (FindVariableFeatures and ScaleData). The scaled matrices were dimensionally reduced to 15 principal components. The data were then subjected to neighbor finding (FindNeighbors, k = 20) and clustering (FindClusters, resolution = 1) and visualized through UMAP with 15 principal components as input. Hair cells and supporting cells were bioinformatically selected based on expression of hair cells and supporting cell markers *Myo6* and *Lfng*, respectively. Hair cells were further subcategorized into striola type I hair cells by co-expression of striola marker *Ocm* and type I marker *Spp*, extrastriola type I hair cells by expression of *Spp* without *Ocm*, and extrastriola type II hair cells by expression of *Anxa4* without *Ocm*.

Mouse crista scRNA-seq data (Wilkerson et al., 2021) was downloaded from NCBI Gene Expression Omnibus (GSE168901). The count matrix was analyzed by R package Seurat (v4.1.0). Matrices were normalized (NormalizeData) and scaled for the top 2000 variable genes

(FindVariableFeatures and ScaleData). The scaled matrices were dimensionally reduced to 15 principal components. The data were then subjected to neighbor finding (FindNeighbors, k = 20) and clustering (FindClusters, resolution = 1) and visualized through UMAP with 15 principal components as input. Hair cells and supporting cells were bioinformatically selected based on expression of hair cell and supporting cell markers *Pou4f3* and *Sparcl1*, respectively. Hair cells were further subcategorized into central hair cells by expression of *Ocm* and peripheral hair cells by expression of *Anxa4*.

Pseudotime analysis

We used the R package Monocle3 (v1.0.1) to predict the pseudo temporal relationships within the integrated scRNA-seq dataset of sensory patches from 36 hpf to 12 mpf. Cell paths were predicted by the learn_graph function of Monocle3. We set the origin of the cell paths based on the enriched distribution of 36 to 48 hpf cells. Hair (all macular hair cells, clusters 0-5) and supporting (macular supporting cells clusters 0 and 6) cell paths were selected separately (choose_cells) to plot hair cells and supporting cell marker expression along pseudotime (plot_genes_in_pseudotime).

Differential gene expression

We utilized *presto* package's differential gene expression function to identify differentially expressed genes among the different cell types. Wilcox rank sum test was performed by the function *wilcox usc.* We then filtered for genes with log2 fold change greater than 0.5 and adjusted p-value less than 0.01. To compare inner ear hair cells to lateral line hair cells, we used the following datasets from GEO: 6-7 dpf lateral line hair cells (GSE144827,Kozak et al., 2020), 4 dpf lateral line hair cells (GSE152859, Ohta et al., 2020), and 5 dpf lateral line hair cells and supporting cells (GSE196211, Baek et al., 2022). Hair cells were selected from datasets by expression of *otofb* and integrated along with our 10x Chromium dataset with Scanorama (Hie

et al., 2019). Gene modules were computed in Monocle3 (v1.0.1) with a q-value cutoff of 1 x e-50.

SAMap analysis for cell type homology

We used the python package SAMap (v1.0.2)(Tarashansky et al., 2021) to correlate gene expression patterns and determine cell type homology between mouse utricle (GSE155966) (Jan et al., 2021) or crista (GSE168901) (Wilkerson et al., 2021) hair cells and supporting cells and our 12 mpf zebrafish inner ear scRNA-seq data. Zebrafish lateral line hair cell sc-RNA data (GSE123241) (Lush et al., 2019) was integrated with our 12 mpf inner ear data using Seurat in order to compare to mice. First, a reciprocal BLAST result of the mouse and zebrafish proteomes was obtained by performing blastp (protein-protein BLAST, NCBI) in both directions using in-frame translated peptide sequences of zebrafish and mouse transcriptome, available from Ensembl (Danio_rerio.GRCz11.pep.all.fa and Mus_musculus.GRCm38.pep.all.fa). The generated maps were then used for the SAMap algorithm. Raw count matrices of zebrafish and mouse scRNA-seq Seurat objects with annotated cell types were converted to h5ad format using SeuratDisk package (v0.0.0.9020) and loaded into Python 3.8.3. Raw data were then processed and integrated by SAMap. Mapping scores between cell types of different species were then calculated by get_mapping_scores and visualized by sankey_plot. Gene pairs driving cell type homology were identified by GenePairFinder.

Data availability

Single-cell RNA seq datasets are available from the NCBI Gene Expression Omnibus with Gene Set Accession number GSE211728.

Acknowledgments

584 This manuscript is dedicated to Neil Segil, who was a wonderful colleague, friend, and mentor to
585 many. We thank Megan Matsutani for fish care, the USC Stem Cell Flow Cytometry Core, and
586 the CHLA Next-Generation Sequencing Core. We also thank David White and the UW Zebrafish
587 Facility staff for fish care.

588

589 **References**

590 Baek, S., Tran, N.T.T., Diaz, D.C., Tsai, Y.-Y., Acedo, J.N., Lush, M.E., Piotrowski, T., 2022.
591 Single-cell transcriptome analysis reveals three sequential phases of gene expression
592 during zebrafish sensory hair cell regeneration. Dev. Cell 57, 799-819.e6.
593 https://doi.org/10.1016/j.devcel.2022.03.001
594 Bhandiwad, A.A., Zeddies, D.G., Raible, D.W., Rubel, E.W., Sisneros, J.A. 2013. Auditory
595 sensitivity of larval zebrafish (Danio rerio) measured using a behavioral prepulse
596 inhibition assay. J Exp Biol. 216, 3504-13. doi: 10.1242/jeb.087635.
597 Cao, J., Spielmann, M., Qiu, X., Huang, X., Ibrahim, D.M., Hill, A.J., Zhang, F., Mundlos, S.,
598 Christiansen, L., Steemers, F.J., Trapnell, C., Shendure, J., 2019. The single-cell
599 transcriptional landscape of mammalian organogenesis. Nature 566, 496–502.
600 https://doi.org/10.1038/s41586-019-0969-x
601 Chang, J.S.Y., Popper, A.N., Saidel, W.M., 1992. Heterogeneity of sensory hair cells in a fish
602 ear. J. Comp. Neurol. 324, 621–640. https://doi.org/10.1002/cne.903240413
603 Chatterjee, P., Padmanarayana, M., Abdullah, N., Holman, C.L., LaDu, J., Tanguay, R.L.,
604 Johnson, C.P., 2015. Otoferlin deficiency in zebrafish results in defects in balance and
605 hearing: rescue of the balance and hearing phenotype with full-length and truncated
606 forms of mouse otoferlin. Mol. Cell. Biol. 35, 1043–1054.
607 https://doi.org/10.1128/MCB.01439-14
608 Choi, H.M.T., Calvert, C.R., Husain, N., Huss, D., Barsi, J.C., Deverman, B.E., Hunter, R.C.,
609 Kato, M., Lee, S.M., Abelin, A.C.T., Rosenthal, A.Z., Akbari, O.S., Li, Y., Hay, B.A.,
610 Sternberg, P.W., Patterson, P.H., Davidson, E.H., Mazmanian, S.K., Prober, D.A., van
611 de Rijn, M., Leadbetter, J.R., Newman, D.K., Readhead, C., Bronner, M.E., Wold, B.,
612 Lansford, R., Sauka-Spengler, T., Fraser, S.E., Pierce, N.A., 2016. Mapping a
613 multiplexed zoo of mRNA expression. Dev. Camb. Engl. 143, 3632–3637.
614 https://doi.org/10.1242/dev.140137
615 Choi, H.M.T., Schwarzkopf, M., Fornace, M.E., Acharya, A., Artavanis, G., Stegmaier, J.,
616 Cunha, A., Pierce, N.A., 2018. Third-generation in situ hybridization chain reaction:
617 multiplexed, quantitative, sensitive, versatile, robust. Dev. Camb. Engl. 145, dev165753.
618 https://doi.org/10.1242/dev.165753
619 Corwin, J.T., Cotanche, D.A., 1988. Regeneration of sensory hair cells after acoustic trauma.
620 Science 240, 1772–1774. https://doi.org/10.1126/science.3381100
621 Cui, G., Meyer, A.C., Calin-Jageman, I., Neef, J., Haeseleer, F., Moser, T., Lee, A. 2007. Ca2+-
622 binding proteins tune Ca2+-feedback to Cav1.3 channels in mouse auditory hair cells. J
623 Physiol. 585, 791-803. doi: 10.1113/jphysiol.2007.142307
624 Curthoys, I.S. 2017. The new vestibular stimuli: sound and vibration-anatomical, physiological
625 and clinical evidence. Exp Brain Res. 235, 957-972. doi: 10.1007/s00221-017-4874-y.
626 Dernedde, J., Weise, C., Müller, E.-C., Hagiwara, A., Bachmann, S., Suzuki, M., Reutter, W.,
627 Tauber, R., Scherer, H., 2014. Cupulin is a zona pellucida-like domain protein and major

628 component of the cupula from the inner ear. PloS One 9, e111917.
629 https://doi.org/10.1371/journal.pone.0111917
630 Desai, S.S., Zeh, C., Lysakowski, A., 2005. Comparative morphology of rodent vestibular
631 periphery. I. Saccular and utricular maculae. J. Neurophysiol. 93, 251–266.
632 https://doi.org/10.1152/jn.00746.2003
633 Di Donato, V., Auer, T.O., Duroure, K., Del Bene, F., 2013. Characterization of the calcium
634 binding protein family in zebrafish. PloS One 8, e53299.
635 https://doi.org/10.1371/journal.pone.0053299
636 Down, M., Power, M., Smith, S.I., Ralston, K., Spanevello, M., Burns, G.F., Boyd, A.W., 2005.
637 Cloning and expression of the large zebrafish protocadherin gene, Fat. Gene Expr.
638 Patterns GEP 5, 483–490. https://doi.org/10.1016/j.modgep.2004.12.005
639 Dutton, K., Abbas, L., Spencer, J., Brannon, C., Mowbray, C., Nikaido, M., Kelsh, R.N.,
640 Whitfield, T.T., 2009. A zebrafish model for Waardenburg syndrome type IV reveals
641 diverse roles for Sox10 in the otic vesicle. Dis. Model. Mech. 2, 68–83.
642 https://doi.org/10.1242/dmm.001164
643 Eatock, R.A., Songer, J.E., 2011. Vestibular hair cells and afferents: two channels for head
644 motion signals. Annu. Rev. Neurosci. 34, 501–534. https://doi.org/10.1146/annurev-
645 neuro-061010-113710
646 Erickson, T., Nicolson, T., 2015. Identification of sensory hair-cell transcripts by thiouracil-
647 tagging in zebrafish. BMC Genomics 16, 842. https://doi.org/10.1186/s12864-015-2072-
648 5
649 Erickson, T., Pacentine, I.V., Venuto, A., Clemens, R., Nicolson, T., 2019. The lhfpl5 Ohnologs
650 lhfpl5a and lhfpl5b Are Required for Mechanotransduction in Distinct Populations of
651 Sensory Hair Cells in Zebrafish. Front. Mol. Neurosci. 12, 320.
652 https://doi.org/10.3389/fnmol.2019.00320
653 Ernest, S., Rauch, G.J., Haffter, P., Geisler, R., Petit, C., Nicolson, T., 2000. Mariner is defective
654 in myosin VIIA: a zebrafish model for human hereditary deafness. Hum. Mol. Genet. 9,
655 2189–2196. https://doi.org/10.1093/hmg/9.14.2189
656 Fabian, P., Tseng, K.-C., Thiruppathy, M., Arata, C., Chen, H.-J., Smeeton, J., Nelson, N.,
657 Crump, J.G., 2022. Lifelong single-cell profiling of cranial neural crest diversification in
658 zebrafish. Nat. Commun. 13, 13. https://doi.org/10.1038/s41467-021-27594-w
659 Favre-Bulle, I.A., Taylor, M.A., Marquez-Legorreta, E., Vanwalleghem, G., Poulsen, R.E.,
660 Rubinsztein-Dunlop, H., Scott, E.K., 2020. Sound generation in zebrafish with Bio-Opto-
661 Acoustics. Nat. Commun. 11, 6120. https://doi.org/10.1038/s41467-020-19982-5
662 Feng, Y., Xu, Q., 2010. Pivotal role of hmx2 and hmx3 in zebrafish inner ear and lateral line
663 development. Dev. Biol. 339, 507–518. https://doi.org/10.1016/j.ydbio.2009.12.028
664 Golub, J.S., Tong, L., Ngyuen, T.B., Hume, C.R., Palmiter, R.D., Rubel, E.W., Stone, J.S., 2012.
665 Hair cell replacement in adult mouse utricles after targeted ablation of hair cells with
666 diphtheria toxin. J. Neurosci. Off. J. Soc. Neurosci. 32, 15093–15105.
667 https://doi.org/10.1523/JNEUROSCI.1709-12.2012
668 Goodyear, R.J., Lu, X., Deans, M.R., Richardson, G.P., 2017. A tectorin-based matrix and
669 planar cell polarity genes are required for normal collagen-fibril orientation in the
670 developing tectorial membrane. Dev. Camb. Engl. 144, 3978–3989.
671 https://doi.org/10.1242/dev.151696
672 Haas, P., Gilmour, D., 2006. Chemokine signaling mediates self-organizing tissue migration in
673 the zebrafish lateral line. Dev. Cell 10, 673–680.
674 https://doi.org/10.1016/j.devcel.2006.02.019
675 Haddon, C., Jiang, Y.J., Smithers, L., Lewis, J. 1998. Delta-Notch signalling and the patterning
676 of sensory cell differentiation in the zebrafish ear: evidence from the mind bomb mutant.
677 Development. 125, 4637-44. doi: 10.1242/dev.125.23.4637.

678 Haden, M., Einarsson, R., Yazejian, B., 2013. Patch clamp recordings of hair cells isolated from
679 zebrafish auditory and vestibular end organs. Neuroscience 248, 79–87.
680 https://doi.org/10.1016/j.neuroscience.2013.05.062
681 Hailey, D.W., Esterberg, R., Linbo, T.H., Rubel, E.W., Raible, D.W., 2017. Fluorescent
682 aminoglycosides reveal intracellular trafficking routes in mechanosensory hair cells. J.
683 Clin. Invest. 127, 472–486. https://doi.org/10.1172/JCI85052
684 Hao, Y., Hao, S., Andersen-Nissen, E., Mauck, W.M., Zheng, S., Butler, A., Lee, M.J., Wilk,
685 A.J., Darby, C., Zager, M., Hoffman, P., Stoeckius, M., Papalexi, E., Mimitou, E.P., Jain,
686 J., Srivastava, A., Stuart, T., Fleming, L.M., Yeung, B., Rogers, A.J., McElrath, J.M.,
687 Blish, C.A., Gottardo, R., Smibert, P., Satija, R., 2021. Integrated analysis of multimodal
688 single-cell data. Cell 184, 3573-3587.e29. https://doi.org/10.1016/j.cell.2021.04.048
689 Hie, B., Bryson, B., Berger, B., 2019. Efficient integration of heterogeneous single-cell
690 transcriptomes using Scanorama. Nat. Biotechnol. 37, 685–691.
691 https://doi.org/10.1038/s41587-019-0113-3
692 Hoffman, L.F., Choy, K.R., Sultemeier, D.R., Simmons, D.D., 2018. Oncomodulin Expression
693 Reveals New Insights into the Cellular Organization of the Murine Utricle Striola. J.
694 Assoc. Res. Otolaryngol. JARO 19, 33–51. https://doi.org/10.1007/s10162-017-0652-6
695 Holt, J.R., Stauffer, E.A., Abraham, D., Géléoc, G.S.G., 2007. Dominant-negative inhibition of
696 M-like potassium conductances in hair cells of the mouse inner ear. J. Neurosci. Off. J.
697 Soc. Neurosci. 27, 8940–8951. https://doi.org/10.1523/JNEUROSCI.2085-07.2007
698 Jan, T.A., Eltawil, Y., Ling, A.H., Chen, L., Ellwanger, D.C., Heller, S., Cheng, A.G., 2021.
699 Spatiotemporal dynamics of inner ear sensory and non-sensory cells revealed by single-
700 cell transcriptomics. Cell Rep. 36, 109358. https://doi.org/10.1016/j.celrep.2021.109358
701 Jiang, M., Karasawa, T., Steyger, P.S., 2017. Aminoglycoside-Induced Cochleotoxicity: A
702 Review. Front. Cell. Neurosci. 11, 308. https://doi.org/10.3389/fncel.2017.00308
703 Jimenez, E., Slevin, C.C., Colón-Cruz, L., Burgess, S.M., 2021. Vestibular and Auditory Hair
704 Cell Regeneration Following Targeted Ablation of Hair Cells With Diphtheria Toxin in
705 Zebrafish. Front. Cell. Neurosci. 15, 721950. https://doi.org/10.3389/fncel.2021.721950
706 Jimenez, E., Slevin, C.C., Song, W., Chen, Z., Frederickson, S.C., Gildea, D., Wu, W.,
707 Elkahloun, A.G., Ovcharenko, I., Burgess, S.M., 2022. A regulatory network of Sox and
708 Six transcription factors initiate a cell fate transformation during hearing regeneration in
709 adult zebrafish. Cell Genomics 2, 100170. https://doi.org/10.1016/j.xgen.2022.100170.
710 Kague, E., Gallagher, M., Burke, S., Parsons, M., Franz-Odendaal, T., Fisher, S., 2012.
711 Skeletogenic Fate of Zebrafish Cranial and Trunk Neural Crest. PLoS ONE 7, e47394.
712 https://doi.org/10.1371/journal.pone.0047394
713 Kalka, M., Markiewicz, N., Ptak, M., Sone, E.D., Ożyhar, A., Dobryszycki, P., Wojtas, M., 2019.
714 In vivo and in vitro analysis of starmaker activity in zebrafish otolith biomineralization.
715 FASEB J. Off. Publ. Fed. Am. Soc. Exp. Biol. 33, 6877–6886.
716 https://doi.org/10.1096/fj.201802268R
717 Kharkovets, T., Hardelin, J.P., Safieddine, S., Schweizer, M., El-Amraoui, A., Petit, C., Jentsch,
718 T.J., 2000. KCNQ4, a K+ channel mutated in a form of dominant deafness, is expressed
719 in the inner ear and the central auditory pathway. Proc. Natl. Acad. Sci. U. S. A. 97,
720 4333–4338. https://doi.org/10.1073/pnas.97.8.4333
721 Kozak, E.L., Palit, S., Miranda-Rodríguez, J.R., Janjic, A., Böttcher, A., Lickert, H., Enard, W.,
722 Theis, F.J., López-Schier, H., 2020. Epithelial Planar Bipolarity Emerges from Notch-
723 Mediated Asymmetric Inhibition of Emx2. Curr. Biol. CB 30, 1142-1151.e6.
724 https://doi.org/10.1016/j.cub.2020.01.027
725 Lapeyre, P., Guilhaume, A., Cazals, Y., 1992. Differences in hair bundles associated with type I
726 and type II vestibular hair cells of the guinea pig saccule. Acta Otolaryngol. (Stockh.)
727 112, 635–642. https://doi.org/10.3109/00016489209137453

Lee, S.G., Huang, M., Obholzer, N.D., Sun, S., Li, W., Petrillo, M., Dai, P., Zhou, Y., Cotanche, D.A., Megason, S.G., Li, H., Chen, Z.-Y., 2016. Myc and Fgf Are Required for Zebrafish Neuromast Hair Cell Regeneration. PloS One 11, e0157768. https://doi.org/10.1371/journal.pone.0157768

Li, A., Xue, J., Peterson, E.H., 2008. Architecture of the mouse utricle: macular organization and hair bundle heights. J. Neurophysiol. 99, 718–733. https://doi.org/10.1152/jn.00831.2007

Liu, Z., Hildebrand, D.G.C., Morgan, J.L., Jia, Y., Slimmon, N., Bagnall, M.W., 2022. The organization of the gravity-sensing system in zebrafish. https://doi.org/10.1101/2021.07.09.451839

Lush, M.E., Diaz, D.C., Koenecke, N., Baek, S., Boldt, H., St Peter, M.K., Gaitan-Escudero, T., Romero-Carvajal, A., Busch-Nentwich, E.M., Perera, A.G., Hall, K.E., Peak, A., Haug, J.S., Piotrowski, T., 2019. scRNA-Seq reveals distinct stem cell populations that drive hair cell regeneration after loss of Fgf and Notch signaling. eLife 8, e44431. https://doi.org/10.7554/eLife.44431

Lysakowski, A., Goldberg, J.M., 2004. Morphophysiology of the vestibular periphery. Highstein Stephen M Repr. Author Fay Richard R Popper Arthur N Vestib. Syst. 57–152.

McGraw, H.F., Drerup, C.M., Culbertson, M.D., Linbo, T., Raible, D.W., Nechiporuk, A.V., 2011. Lef1 is required for progenitor cell identity in the zebrafish lateral line primordium. Dev. Camb. Engl. 138, 3921–3930. https://doi.org/10.1242/dev.062554

Meredith, F.L., Rennie, K.J., 2016. Channeling your inner ear potassium: K(+) channels in vestibular hair cells. Hear. Res. 338, 40–51. https://doi.org/10.1016/j.heares.2016.01.015

Millimaki, B.B., Sweet, E.M., Dhason, M.S., Riley, B.B., 2007. Zebrafish atoh1 genes: classic proneural activity in the inner ear and regulation by Fgf and Notch. Dev. Camb. Engl. 134, 295–305. https://doi.org/10.1242/dev.02734

Monroe, J.D., Rajadinakaran, G., Smith, M.E., 2015. Sensory hair cell death and regeneration in fishes. Front. Cell. Neurosci. 9. https://doi.org/10.3389/fncel.2015.00131

Moravec, W.J., Peterson, E.H., 2004. Differences Between Stereocilia Numbers on Type I and Type II Vestibular Hair Cells. J. Neurophysiol. 92, 3153–3160. https://doi.org/10.1152/jn.00428.2004

Mosimann, C., Kaufman, C.K., Li, P., Pugach, E.K., Tamplin, O.J., Zon, L.I., 2011. Ubiquitous transgene expression and Cre-based recombination driven by the *ubiquitin* promoter in zebrafish. Development 138, 169–177. https://doi.org/10.1242/dev.059345

Musser, J.M., Schippers, K.J., Nickel, M., Mizzon, G., Kohn, A.B., Pape, C., Ronchi, P., Papadopoulos, N., Tarashansky, A.J., Hammel, J.U., Wolf, F., Liang, C., Hernández-Plaza, A., Cantalapiedra, C.P., Achim, K., Schieber, N.L., Pan, L., Ruperti, F., Francis, W.R., Vargas, S., Kling, S., Renkert, M., Polikarpov, M., Bourenkov, G., Feuda, R., Gaspar, I., Burkhardt, P., Wang, B., Bork, P., Beck, M., Schneider, T.R., Kreshuk, A., Wörheide, G., Huerta-Cepas, J., Schwab, Y., Moroz, L.L., Arendt, D., 2021. Profiling cellular diversity in sponges informs animal cell type and nervous system evolution. Science 374, 717–723. https://doi.org/10.1126/science.abj2949

Obholzer, N., Wolfson, S., Trapani, J.G., Mo, W., Nechiporuk, A., Busch-Nentwich, E., Seiler, C., Sidi, S., Söllner, C., Duncan, R.N., Boehland, A., Nicolson, T., 2008. Vesicular glutamate transporter 3 is required for synaptic transmission in zebrafish hair cells. J. Neurosci. Off. J. Soc. Neurosci. 28, 2110–2118. https://doi.org/10.1523/JNEUROSCI.5230-07.2008

Ohta, S., Ji, Y.R., Martin, D., Wu, D.K., 2020. Emx2 regulates hair cell rearrangement but not positional identity within neuromasts. eLife 9, e60432. https://doi.org/10.7554/eLife.60432

Olt, J., Johnson, S.L., Marcotti, W., 2014. In vivo and in vitro biophysical properties of hair cells from the lateral line and inner ear of developing and adult zebrafish. J. Physiol. 592, 2041–2058. https://doi.org/10.1113/jphysiol.2013.265108

Petko, J.A., Millimaki, B.B., Canfield, V.A., Riley, B.B., Levenson, R., 2008. Otoc1: a novel otoconin-90 ortholog required for otolith mineralization in zebrafish. Dev. Neurobiol. 68, 209–222. https://doi.org/10.1002/dneu.20587

Phillips, J.B., Blanco-Sanchez, B., Lentz, J.J., Tallafuss, A., Khanobdee, K., Sampath, S., Jacobs, Z.G., Han, P.F., Mishra, M., Titus, T.A., Williams, D.S., Keats, B.J., Washbourne, P., Westerfield, M., 2011. Harmonin (Ush1c) is required in zebrafish Müller glial cells for photoreceptor synaptic development and function. Dis. Model. Mech. 4, 786–800. https://doi.org/10.1242/dmm.006429

Picher, M.M., Gehrt, A., Meese, S., Ivanovic, A., Predoehl, F., Jung, S., Schrauwen, I., Dragonetti, A.G., Colombo, R., Van Camp, G., Strenzke, N., Moser, T., 2017. Ca2+-binding protein 2 inhibits Ca2+-channel inactivation in mouse inner hair cells. Proc. Natl. Acad. Sci. U. S. A. 114, E1717–E1726. https://doi.org/10.1073/pnas.1617533114

Pickett, S.B., Raible, D.W., 2019. Water Waves to Sound Waves: Using Zebrafish to Explore Hair Cell Biology. J. Assoc. Res. Otolaryngol. JARO 20, 1–19. https://doi.org/10.1007/s10162-018-00711-1

Platt, C., 1993. Zebrafish inner ear sensory surfaces are similar to those in goldfish. Hear. Res. 65, 133–140. https://doi.org/10.1016/0378-5955(93)90208-i

Popper, A.N., 2000. Hair cell heterogeneity and ultrasonic hearing: recent advances in understanding fish hearing. Philos. Trans. R. Soc. B Biol. Sci. 355, 1277–1280.

Popper, A.N., Fay, R.R., 1993. Sound detection and processing by fish: critical review and major research questions. Brain. Behav. Evol. 41, 14–38. https://doi.org/10.1159/000113821

Postlethwait, J.H., 2007. The zebrafish genome in context: ohnologs gone missing. J. Exp. Zoolog. B Mol. Dev. Evol. 308, 563–577. https://doi.org/10.1002/jez.b.21137

Poulsen RE, Scholz LA, Constantin L, Favre-Bulle I, Vanwalleghem GC, Scott EK. Broad frequency sensitivity and complex neural coding in the larval zebrafish auditory system. Curr Biol. 2021 May 10;31(9):1977-1987.e4. doi: 10.1016/j.cub.2021.01.103.

Privat, M., Romano, S.A., Pietri, T., Jouary, A., Boulanger-Weill, J., Elbaz, N., Duchemin, A., Soares, D., Sumbre, G., 2019. Sensorimotor Transformations in the Zebrafish Auditory System. Curr. Biol. CB 29, 4010-4023.e4. https://doi.org/10.1016/j.cub.2019.10.020

Qian, F., Wei, G., Gao, Y., Wang, Xin, Gong, J., Guo, C., Wang, Xiaoning, Zhang, X., Zhao, J., Wang, C., Xu, M., Hu, Y., Yin, G., Kang, J., Chai, R., Xie, G., Liu, D., 2022. Single-cell RNA-sequencing of zebrafish hair cells reveals novel genes potentially involved in hearing loss. Cell. Mol. Life Sci. CMLS 79, 385. https://doi.org/10.1007/s00018-022-04410-2

Riley, B.B., Chiang, M., Farmer, L., Heck, R., 1999. The deltaA gene of zebrafish mediates lateral inhibition of hair cells in the inner ear and is regulated by pax2.1. Dev. Camb. Engl. 126, 5669–5678. https://doi.org/10.1242/dev.126.24.5669

Riley, B.B., Moorman, S.J. 2000 Development of utricular otoliths, but not saccular otoliths, is necessary for vestibular function and survival in zebrafish. J Neurobiol. 43, 329-37. doi: 10.1002/1097-4695(20000615)43:4<329::aid-neu2>3.0.co;2-h

Rohs, P., Ebert, A.M., Zuba, A., McFarlane, S., 2013. Neuronal expression of fibroblast growth factor receptors in zebrafish. Gene Expr. Patterns GEP 13, 354–361. https://doi.org/10.1016/j.gep.2013.06.006

Rüsch, A., Lysakowski, A., Eatock, R.A., 1998. Postnatal Development of Type I and Type II Hair Cells in the Mouse Utricle: Acquisition of Voltage-Gated Conductances and Differentiated Morphology. J. Neurosci. 18, 7487–7501. https://doi.org/10.1523/JNEUROSCI.18-18-07487.1998

Sahly, I., Andermann, P., Petit, C., 1999. The zebrafish eya1 gene and its expression pattern during embryogenesis. Dev Genes Evol. 209, 399-410. doi: 10.1007/s004270050270.

Saunders, L.M., Srivatsan, S.R., Duran, M., Dorrity, M.W., Ewing, B., Linbo, T., Shendure, J., Raible, D.W., Moens, C.B., Kimelman, D., Trapnell, C., 2022. Deep molecular, cellular and temporal phenotyping of developmental perturbations at whole organism scale. Biorxiv https://doi.org/10.1101/2022.08.04.502764

Schuck, J.B., Smith, M.E. 2009. Cell proliferation follows acoustically-induced hair cell bundle loss in the zebrafish saccule. Hear Res. 253,67-76. doi: 10.1016/j.heares.2009.03.008.

Schrauwen, I., Helfmann, S., Inagaki, A., Predoehl, F., Tabatabaiefar, M.A., Picher, M.M., Sommen, M., Zazo Seco, C., Oostrik, J., Kremer, H., Dheedene, A., Claes, C., Fransen, E., Chaleshtori, M.H., Coucke, P., Lee, A., Moser, T., Van Camp, G. 2012 A mutation in CABP2, expressed in cochlear hair cells, causes autosomal-recessive hearing impairment. Am J Hum Genet. 91,636-45. doi: 10.1016/j.ajhg.2012.08.018.

Seiler, C., Finger-Baier, K.C., Rinner, O., Makhankov, Y.V., Schwarz, H., Neuhauss, S.C.F., Nicolson, T., 2005. Duplicated genes with split functions: independent roles of protocadherin15 orthologues in zebrafish hearing and vision. Dev. Camb. Engl. 132, 615–623. https://doi.org/10.1242/dev.01591

Sheets, L., Holmgren, M., Kindt, K.S., 2021. How Zebrafish Can Drive the Future of Genetic-based Hearing and Balance Research. J. Assoc. Res. Otolaryngol. JARO 22, 215–235. https://doi.org/10.1007/s10162-021-00798-z

Sheets, L., Kindt, K.S., Nicolson, T., 2012. Presynaptic CaV1.3 channels regulate synaptic ribbon size and are required for synaptic maintenance in sensory hair cells. J. Neurosci. Off. J. Soc. Neurosci. 32, 17273–17286. https://doi.org/10.1523/JNEUROSCI.3005-12.2012

Söllner, C., Burghammer, M., Busch-Nentwich, E., Berger, J., Schwarz, H., Riekel, C., Nicolson, T., 2003. Control of Crystal Size and Lattice Formation by Starmaker in Otolith Biomineralization. Science 302, 282–286. https://doi.org/10.1126/science.1088443

Söllner, C., Rauch, G.-J., Siemens, J., Geisler, R., Schuster, S.C., Müller, U., Nicolson, T., Tübingen 2000 Screen Consortium, 2004. Mutations in cadherin 23 affect tip links in zebrafish sensory hair cells. Nature 428, 955–959. https://doi.org/10.1038/nature02484

Steiner, A.B., Kim, T., Cabot, V., Hudspeth, A.J., 2014. Dynamic gene expression by putative hair-cell progenitors during regeneration in the zebrafish lateral line. Proc. Natl. Acad. Sci. U. S. A. 111, E1393-1401. https://doi.org/10.1073/pnas.1318692111

Stone, J.S., Cotanche, D.A., 2007. Hair cell regeneration in the avian auditory epithelium. Int. J. Dev. Biol. 51, 633–647. https://doi.org/10.1387/ijdb.072408js

Stooke-Vaughan, G.A., Obholzer, N.D., Baxendale, S., Megason, S.G., Whitfield, T.T., 2015. Otolith tethering in the zebrafish otic vesicle requires Otogelin and α-Tectorin. Dev. Camb. Engl. 142, 1137–1145. https://doi.org/10.1242/dev.116632

Tarashansky, A.J., Musser, J.M., Khariton, M., Li, P., Arendt, D., Quake, S.R., Wang, B., 2021. Mapping single-cell atlases throughout Metazoa unravels cell type evolution. eLife 10, e66747. https://doi.org/10.7554/eLife.66747

Thomas, E.D., Raible, D.W., 2019. Distinct progenitor populations mediate regeneration in the zebrafish lateral line. eLife 8, e43736. https://doi.org/10.7554/eLife.43736

Vijayakumar, S., Jones, S.M., Jones, T.A., Tian, C., Johnson, K.R., 2019. Spontaneous mutations of the Zpld1 gene in mice cause semicircular canal dysfunction but do not impair gravity receptor or hearing functions. Sci. Rep. 9, 12430. https://doi.org/10.1038/s41598-019-48835-5

Wilkerson, B.A., Zebroski, H.L., Finkbeiner, C.R., Chitsazan, A.D., Beach, K.E., Sen, N., Zhang, R.C., Bermingham-McDonogh, O., 2021. Novel cell types and developmental lineages revealed by single-cell RNA-seq analysis of the mouse crista ampullaris. eLife 10, e60108. https://doi.org/10.7554/eLife.60108

879 Wolf, F.A., Hamey, F.K., Plass, M., Solana, J., Dahlin, J.S., Göttgens, B., Rajewsky, N., Simon,
880 L., Theis, F.J., 2019. PAGA: graph abstraction reconciles clustering with trajectory
881 inference through a topology preserving map of single cells. Genome Biol. 20, 59.
882 https://doi.org/10.1186/s13059-019-1663-x
883 Xu, P., Balczerski, B., Ciozda, A., Louie, K., Oralova, V., Huysseune, A., Crump, J.G., 2018.
884 Fox proteins are modular competency factors for facial cartilage and tooth specification.
885 Dev. Camb. Engl. 145, dev165498. https://doi.org/10.1242/dev.165498
886 Xue, J., Peterson, E.H., 2006. Hair bundle heights in the utricle: differences between macular
887 locations and hair cell types. J. Neurophysiol. 95, 171–186.
888 https://doi.org/10.1152/jn.00800.2005
889 Yamasoba, T., Kondo, K., 2006. Supporting cell proliferation after hair cell injury in mature
890 guinea pig cochlea in vivo. Cell Tissue Res. 325, 23–31. https://doi.org/10.1007/s00441-
891 006-0157-9
892 Yang, C.-H., Cheng, C.-H., Chen, G.-D., Liao, W.-H., Chen, Y.-C., Huang, K.-Y., Hwang, P.-P.,
893 Hwang, S.-P.L., Huang, C.-J., 2011. Zona Pellucida Domain-Containing Protein β-
894 Tectorin is Crucial for Zebrafish Proper Inner Ear Development. PLOS ONE 6, e23078.
895 https://doi.org/10.1371/journal.pone.0023078
896 Yao, Q., DeSmidt, A.A., Tekin, M., Liu, X., Lu, Z., 2016. Hearing Assessment in Zebrafish
897 During the First Week Postfertilization. Zebrafish 13, 79–86.
898 https://doi.org/10.1089/zeb.2015.1166
899 Yu, R., Wang, P., Chen, X.-W., 2020. The role of gfi1.2 in the development of zebrafish inner
900 ear. Hear. Res. 396, 108055. https://doi.org/10.1016/j.heares.2020.108055
901 Zeddies, DG., Fay, RR. 2005. Development of the acoustically evoked behavioral response in
902 zebrafish to pure tones. J Exp Biol. 208, 1363-72. doi: 10.1242/jeb.01534.
903

Figures & Figure Legends

Figure 1. Anatomy of zebrafish and mouse inner ears
A) Illustration of the lateral line system of a 5 dpf zebrafish. Blue circles represent individual neuromasts located on the body of the fish. Boxed region indicates location of the ear. B) Enlarged diagram of the 5 dpf zebrafish ear showing cristae (red) and macular (blue) sensory organs. C,D) Illustrations of adult zebrafish and mouse inner ears showing homologous end organs in the semicircular canal crista ampullaris (red) and macula otolith organs (blue). Light green and dark green represent unique end organs of the lagena in zebrafish and cochlea in mice. E) Illustration of the mouse utricle showing striolar and extrastriolar regions of the sensory organ. Arrows represent hair cell planar polarity within the sensory organ and red dashed line represents the line of polarity reversal within the striola. ac: anterior crista, c: cochlea, l: lagena, lc: lateral crista, o: otolith, pc: posterior crista, s: saccule, u: utricle.

Figure 2. Molecularly distinct cell types between the zebrafish inner ear and lateral line
Ear and lateral line cells were selected from a whole-embryo single-nucleus RNA-seq dataset from animals between 18 and 96 hpf using known marker genes for hair cells and supporting cells. A-B) UMAP projection of inner ear and lateral line cells grouped by A) developmental timepoint and B) broad cell type: ear nonsensory SC (red), lateral line nonsensory SC (green), ear HC (blue), and lateral line HC (yellow). Clusters in B) correspond to columns of following gene expression plots. Widely accepted marker genes for C) inner ear nonsensory cells, D) lateral line nonsensory cells, and E) hair cells show enriched expression in the corresponding clusters from B, confirming their identity. F) Expression of previously identified marker genes for inner ear or lateral line hair cells was used to identify hair cell origin.

Figure 3. Cell subtypes in the zebrafish inner ear end organs
A-D) Integration and analysis of single-cell RNAseq data generated by sci-Seq (sci) or 10x Chromium sequencing (10x) for inner ear hair cells and supporting cells from embryonic (sci), larval (sci,10x), and adult (10x) stages. UMAP projection of cells are grouped by A) dataset of origin and B) timepoint. C) Unsupervised clustering divides cells into 10 clusters that were grouped into 9 cell subtypes. D) Feature plots showing hair cell marker *myo6b*, nascent hair cell marker *dla*, supporting cell marker *lfng*, and putative progenitor marker *fgfr2* expression in the integrated dataset. E) Differentially expressed genes across the 10 cell clusters.

Figure 4. Pseudotime analysis reveals developmental trajectories in the zebrafish inner ear
A,B) Pseudotime analysis of macular cells showing simulated developmental trajectories of a putative bipotent progenitor population into hair cell and supporting cell clusters. C,D) Changes in putative progenitor markers along C) hair cell and D) supporting cell trajectories. *fat1a* and *pard3bb* only decrease along the hair cell trajectory, while *fgfr2* and *igsf3* decrease along both hair cell and supporting cell trajectories. E) Transient expression of early hair cell genes *dla* and *atoh1a* along hair cell trajectories. F) Increases in gene expression levels of *gfi1aa* and *myo6b* along hair cell trajectories. G) Increases in *stm* and *lfng* along supporting cell trajectories.

Figure 5. Distinct markers separate macula and crista supporting cells
A) Feature plots showing expression of macula supporting cell marker *tectb* and crista supporting cell marker *zpld1a*. B-D) HCR in situ hybridization in myo6b:GFP transgenic animals. Each set of images shown represents a projection of one z-stack split into cristae (lateral) and macula (medial) slices. Lateral line neuromasts positioned over the ear are visible in lateral slices. Expression pattern for B) the pan-supporting cell marker *lfng*, C) macula-specific marker *tectb*, and D) crista-specific marker *zpld1a* in 5 dpf myo6b:GFP fish. Each set of images shown represents a projection of one z-stack split into cristae (lateral) and macula (medial) slices. ac: anterior crista, lc: lateral crista, nm: neuromast, pc: posterior crista, u: utricle, s: saccule. Scale bars = 20 µm.

Figure 6. *cabp1b*+ and *cabp2b*+ label hair cells in distinct regions of sensory end organs
A) Feature plots showing differential expression of *cabp1b* and *cabp2b* among crista and macula hair cells. B-D) HCR in situ projections of individual sensory patches from 5 dpf myo6:GFP fish showing differential spatial expression patterns of *cabp1b* and *cabp2b*. B) *cabp1b* is expressed at the ends of the cristae, while *cabp2b* is expressed centrally. Anterior crista is shown. C) In the utricle, *cabp1b* is expressed medially and *cabp2b* is expressed laterally. D) In the saccule, *cabp1b* is expressed in peripheral cells at the dorsal and ventral edges of the organ. *cabp2b* is expressed centrally. Scale bars for HCR images = 10 µm. E) Cartoon illustrations of the zebrafish utricle, saccule, and lagena, and the expression patterns of *cabp1b* (yellow) and *cabp2b* (magenta) within each sensory patch. F-H) Whole mount RNAScope confocal images of adult inner ear organs showing peripheral expression pattern of *cabp1b* (n = 3) in the adult zebrafish F) utricle, G) saccule, and H) lagena. I-K) Whole mount RNAScope confocal images showing central expression pattern of *cabp2b* (n = 4) in the adult zebrafish I) utricle, J) saccule, and K) lagena. Scale bars for RNAScope images = 25 µm.

Figure 7. Distinct markers separate macula and crista hair cells
A) Feature plots showing marker genes enriched in organ-specific subsets of inner ear hair cells: *cabp5b*, *skor2*, and *loxhd1b* . B-D) HCR in situs in 5 dpf myo6b:GFP fish show expression of B) *cabp5b* in crista but not macula hair cells, C) *skor2* in the utricle only, and D) *loxhd1b* in the saccule, as well as lateral line neuromast hair cells. Each set of images represents an orthogonal projection of one z-stack split into cristae (lateral) and macular (medial) slices. ac: anterior crista, lc: lateral crista, nm: neuromast, pc: posterior crista, s: saccule, u: utricle. Scale bar = 20 µm.

Figure 8. Zebrafish *cabp2b*+ domain shares features with the mouse striolar region
A) Feature plot shows enrichment for the striola marker *pvalb9* in *cabp2b*-expressing striolar cells. B-D) HCR in situs in 5 dpf myo6b:GFP fish shows *pvalb9* and *cabp2b* co-expression in the utricle. Scale bar = 10 µm. E) Cartoon illustration of overlapping expression of *pvalb9* (white) and *cabp2b* (magenta) that coincides with the line of hair cell polarity reversal. F,G) Whole-mount RNAScope confocal images of adult zebrafish utricles showing expression of *pvalb9* relative to F) *cabp1b* (n = 3) and G) *cabp2b* (n = 4). Scale bar = 25 µm. H,I) Whole-mount RNAScope RNA and protein co-detection assay showing co-localization of *cabp2b* expression

(RNA) and the hair cell line of polarity reversal indicated by Spectrin (protein) staining (n = 3). Scale bar = 25 μm. Arrows denote hair cell polarity and dotted line outlines line of polarity reversal.

Figure 9. SAMap analysis reveals conserved gene expression patterns between mouse and zebrafish hair cell types

A-B) Sankey plot showing the SAMap mapping scores (0-1) that indicate transcriptome relatedness between A) mouse utricular and zebrafish macular single-cell clusters and B) mouse and zebrafish cristae single-cell clusters. A mapping score of 0 indicates no evolutionary correlation in transcriptome while a mapping score of 1 indicates perfect correlation. Correlations below 0.15 were not plotted.

Figure 2-figure supplement 1: Gene modules for embryonic to larval inner ear and lateral line dataset

Gene modules calculated in Monocle 3 for the embryonic to larval inner ear and lateral line dataset displayed as A) a heatmap of module gene enrichment by cluster where red indicates higher enrichment and blue indicates de-enrichment and B) module expression across the UMAP for the dataset. Module genes with statistical values are listed in Supplementary File 2.

Figure 2-figure supplement 2. Selection of otic sensory cells from snRNA-seq dataset

A) Clustering of 18 hpf to 96 hpf dataset to illustrate cell subtypes. PAGA analysis of this dataset shows strong connectivity among ear nonsensory cells and among lateral line nonsensory cells, but weak interconnectivity between these two groups. B) Feature plots show expression of the supporting cell marker *lfng*, and markers of structural otic cells *matn4* and *col2a1a*. C) UMAP of sensory patch cells from 36-96hpf are-clustered without structural and early otic vesicle cells. PAGA analysis again shows strong connectivity within hair cells and supporting cell groups and weak connectivity between lateral line and inner ear supporting cells. PAGA connectivity scores are listed in Supplementary File 1.

Figure 2-figure supplement 3. Gene expression differences between lateral line and inner ear hair cells

A) UMAP of our 12 mpf hair cell dataset integrated by Scanorama with published lateral line hair cell datasets. Lateral line hair cells cluster separately from inner ear hair cells. B) Differential gene expression analysis identifies novel marker genes specific to either lateral line or inner ear hair cells.

Figure 3-figure supplement 1. scRNA-seq of 12 mpf zebrafish inner ear captures sensory hair cells and supporting cells as well as non-sensory supporting cells

A) Clustering of 12 mpf dataset to illustrate cell types in the adult zebrafish inner ear. B-I) Feature plots of 12 mpf zebrafish scRNA-seq dataset alone showing expression of hair cell markers B) *myo6b* and C) *strc*, pan-supporting cell marker D) *stm*, sensory supporting cell markers E) *lfng* and F) *hey1*, and pan-otic marker G) *otomp*, and non-sensory supporting cell markers H) *matn4* and I) *col2a1a*.

Figure 3-figure supplement 2. Hair cell and supporting cell marker expression in the integrated scRNA-seq dataset

Feature plots of integrated zebrafish scRNA-seq datasets showing expression of nascent hair cell marker A) *atoh1a,* inner ear hair cell markers B) *strc,* C) *gfi1aa*, and D) *lhfpl5a*, and pan-supporting cell marker E) *stm*.

Figure 3-figure supplement 3. Putative progenitor marker expression in individual progenitor and supporting cell clusters

A) Combined and individual UMAP projections of putative bipotent progenitor cluster (cluster 0), macular supporting cell cluster (cluster 6), and cristae supporting cell cluster (cluster 7) from the integrated zebrafish inner ear dataset. B-E) Feature plots show expression of putative progenitor genes in the integrated dataset, as well as in individual clusters of 0, 6, and 7. F) Violin plots showing differential gene expression of *fgfr2*, *igsf3*, *fat1a*, and *pard3bb* among clusters 0, 6, and 7. Wilcoxon rank sum test, *: p <= 0.05, ***: p <= 1e-3, ****: p <= 1e-4.

Figure 3-figure supplement 4: Gene modules for integrated inner ear sensory patch dataset

Gene modules calculated in Monocle 3 for the integrated inner ear sensory patch dataset displayed as A) a heatmap of module gene enrichment by cluster where red indicates higher enrichment and blue indicates de-enrichment and B) module expression across the UMAP for the dataset. Module genes with statistical values are listed in Supplementary File 5.

Figure 4-figure supplement 1. Pseudotime analysis of cristae hair and supporting cells in the zebrafish inner ear

A) Pseudotime analysis showing simulated developmental trajectories of a putative bipotent progenitor population into both cristae hair and supporting cell clusters. B,C) Changes in putative progenitor markers along B) hair cell and C) supporting cell trajectories. *fat1a* and *pard3bb* only decrease along the hair cell trajectory, while *fgfr2* and *igsf3* decrease along both hair cell and supporting cell trajectories. D) Transient expression of early hair cell genes *dla* and *atoh1a* along hair cell trajectories. E) Increases in gene expression levels of *gfi1aa* and *myo6b* along hair cell trajectories. F) Increases in *stm* and *lfng* along supporting cell trajectories.

Figure 4-figure supplement 2: *dla* labels putative hair cell progenitors in the cristae and maculae

HCR in situ hybridization of 5 dpf zebrafish. Maximum intensity projections of A) posterior crista (lateral view), B) utricle (dorsal view), and C) saccule (lateral view) showing *dla* expression in a subset of support cells (arrowheads) peripheral to *myo6b*+ hair cells. Scale bars = 10 µm.

Figure 5-figure supplement 1. *zpld1a* and *tectb* are primarily expressed in supporting cells

HCR in situ hybridization of 5 dpf myo6b:GFP zebrafish. A-B) Confocal slices through A) anterior crista and B) lateral crista (lateral view) show localization of *cabp5b* in hair cells and *zpld1a* in supporting cells. C) Slice through utricle (dorsal view) shows *cabp2b* expression in hair cells and *tectb* expression primarily in the surrounding supporting cells. D) Slices through

saccule (lateral view) at the level of hair cell bodies (top row) and supporting cell bodies (bottom row). *cabp2b* is primarily expressed in hair cells and *tectb* is primarily expressed in supporting cells. Scale bars = 10 µm.

Figure 7-figure supplement 1. *skor2* and *loxhd1b* label subsets of hair cells in utricle or saccule

HCR in situ hybridization of 5 dpf zebrafish. A) Maximum intensity projection of utricle (dorsal view) showing *skor2* expression in medially located hair cells. B) Maximum intensity projection of saccule (lateral view) showing *loxhd1b* expression in a peripheral subset of hair cells. Scale bars = 10 µm.

Figure 8-figure supplement 1. Striola marker *pvalb9* is expressed in all inner ear sensory end organs

HCR in situ hybridization of 5 dpf zebrafish. A) Maximum intensity projection of saccule (lateral view) shows *pvalb9* expression in centrally located hair cells. B) Slice through the anterior crista shows *pvalb9* expression in a subset of crista hair cells. Scale bars = 10 µm.

Figure 8-figure supplement 2. Inner ear hair cell subtypes differentially express mechanosensory apparatus genes

Feature plots for mechanosensory transduction genes from the integrated zebrafish scRNA-seq dataset of Figure 3.

Figure 8-figure supplement 3. Inner ear hair cell subtypes differentially express voltage-gated calcium and potassium channel genes

Feature plots for ion channel genes from the integrated zebrafish scRNA-seq dataset of Figure 3.

Figure 9-figure supplement 1. SAMap analysis of mouse utricle versus zebrafish macular and lateral line cells

A-B) Sankey plot showing the SAMap mapping scores (0-1) that indicate transcriptome relatedness between mouse utricular and integrated zebrafish macular and lateral line single-cell clusters. A) Zebrafish 12 mpf macular HCs integrated with 5 dpf lateral line HCs. B) Zebrafish 3-5 dpf macular HCs integrated with 5 dpf lateral line HCs. A mapping score of 0 indicates no evolutionary correlation in transcriptome, and a mapping score of 1 indicates perfect correlation. Correlations below 0.2 were not plotted.

List of Files

Supplementary File 1: Differentially expressed genes across inner ear and lateral line clusters

Supplementary File 2. PAGA scores for relative connectivity between clusters (related to Supplementary Figure 1)

Supplementary File 3. Gene modules for embryonic to larval inner ear and lateral line dataset

Supplementary File 4. Differentially expressed genes in inner ear cell clusters

Supplementary File 5. Gene modules for inner ear sensory patch dataset

Supplementary File 6. Genes enriched along pseudotime trajectories

Supplementary File 7. Genes enriched in supporting cell clusters

Supplementary File 8. Genes enriched in *cabp1b*+ and *cabp2b*+ macular cells

Supplementary File 9. Genes driving macular SAMap alignment

Supplementary File10. Genes enriched in *cabp1b*+ and *cabp2b*+ crista cells

Supplementary File 11. Genes driving crista SAMap alignment

Supplementary File 12. cDNA sequences used for HCR in situ hybridization probes

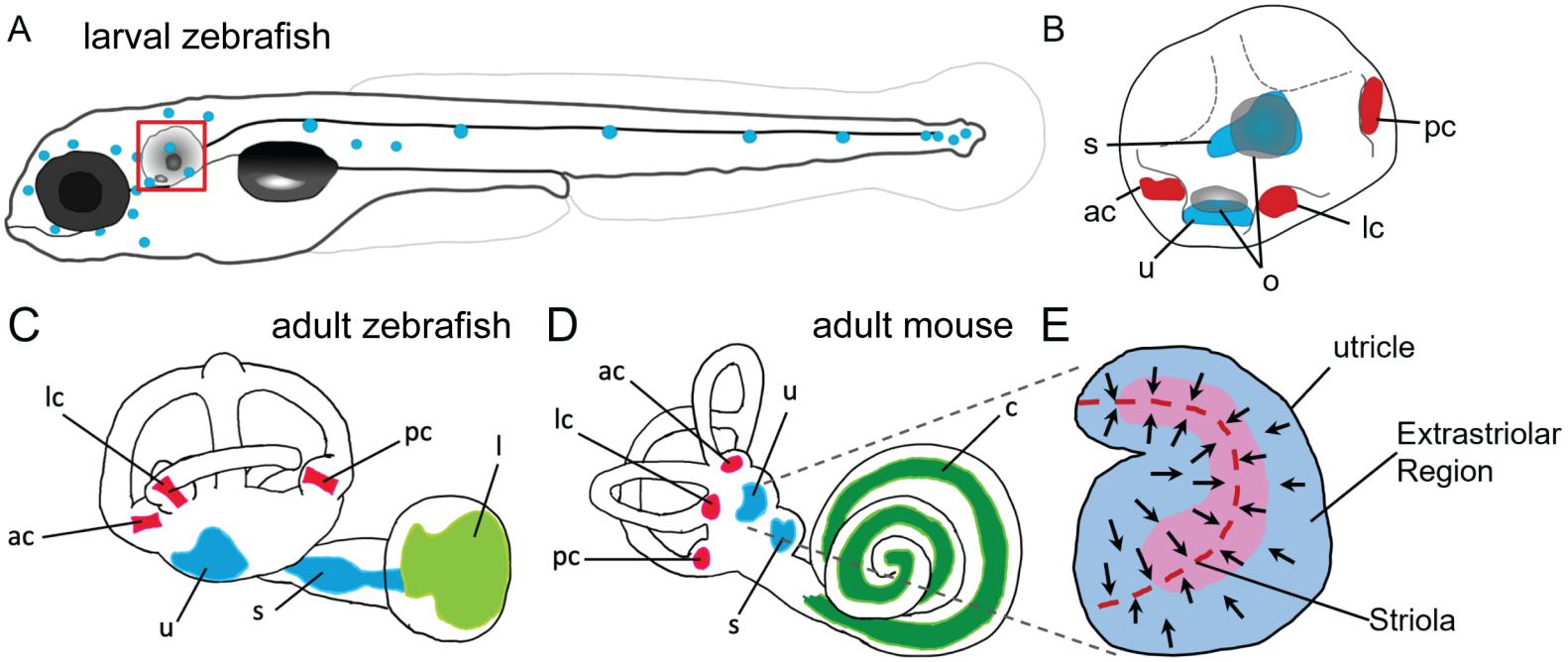
A
larval zebrafish
B
s
pc
ac
lc
u
o
C
adult zebrafish
lc
pc
l
ac
u
s
D
adult mouse
ac
u
lc
c
pc
s
E
utricle
Extrastriolar
Region
Striola

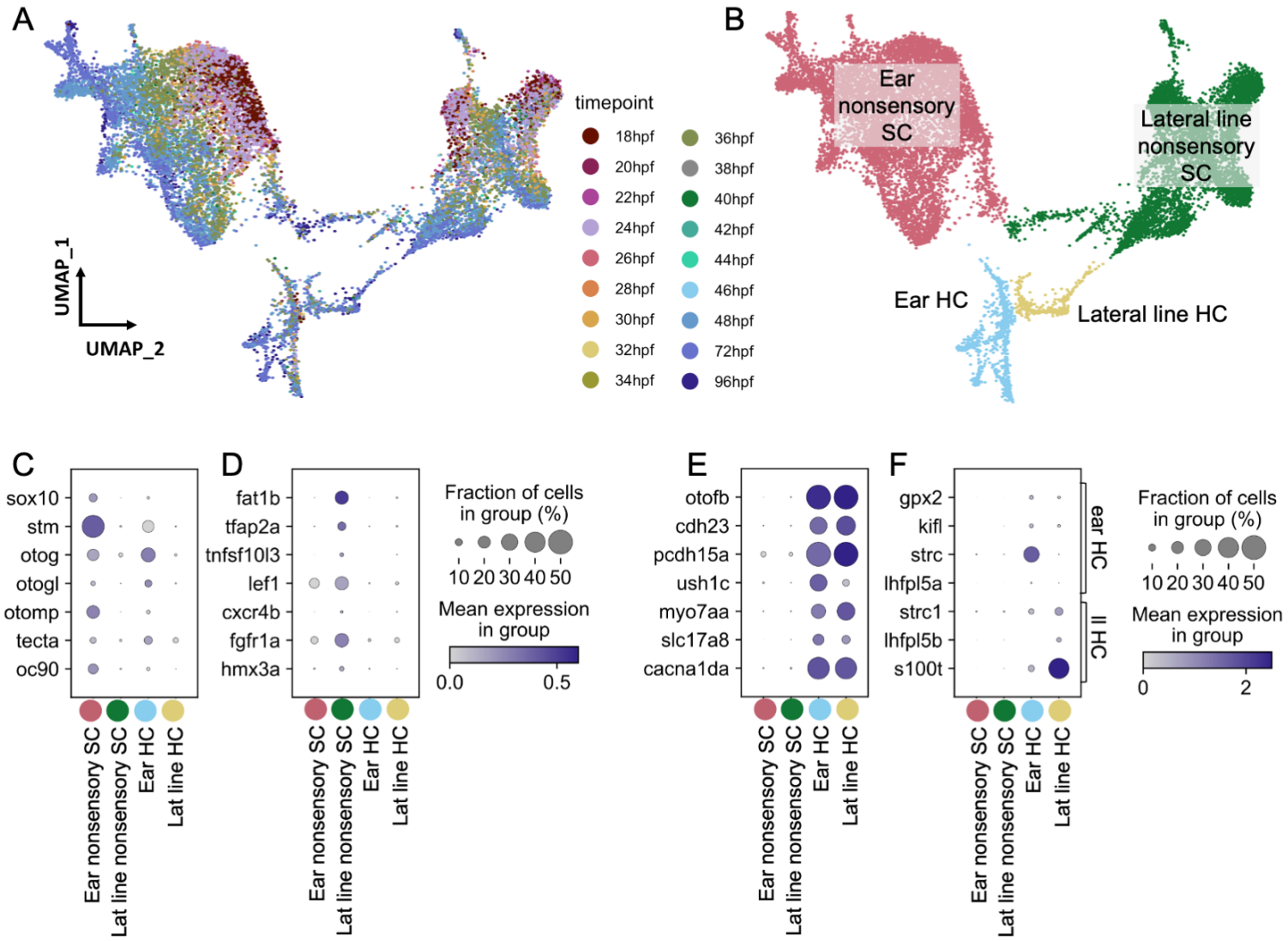
A
UMAP_1
UMAP_2
timepoint
18hpf
20hpf
22hpf
24hpf
26hpf
28hpf
30hpf
32hpf
34hpf
36hpf
38hpf
40hpf
42hpf
44hpf
46hpf
48hpf
72hpf
96hpf
B
Ear nonsensory SC
Lateral line nonsensory SC
Ear HC
Lateral line HC
C
sox10
stm
otog
otogl
otomp
tecta
oc90
D
fat1b
tfap2a
tnfsf10l3
lef1
cxcr4b
fgfr1a
hmx3a
Fraction of cells in group (%)
10 20 30 40 50
Mean expression in group
0.0
0.5
E
otofb
cdh23
pcdh15a
ush1c
myo7aa
slc17a8
cacna1da
F
gpx2
kifl
strc
lhfpl5a
strc1
lhfpl5b
s100t
ear HC
II HC
Fraction of cells in group (%)
10 20 30 40 50
Mean expression in group
0
2
Ear nonsensory SC
Lat line nonsensory SC
Ear HC
Lat line HC

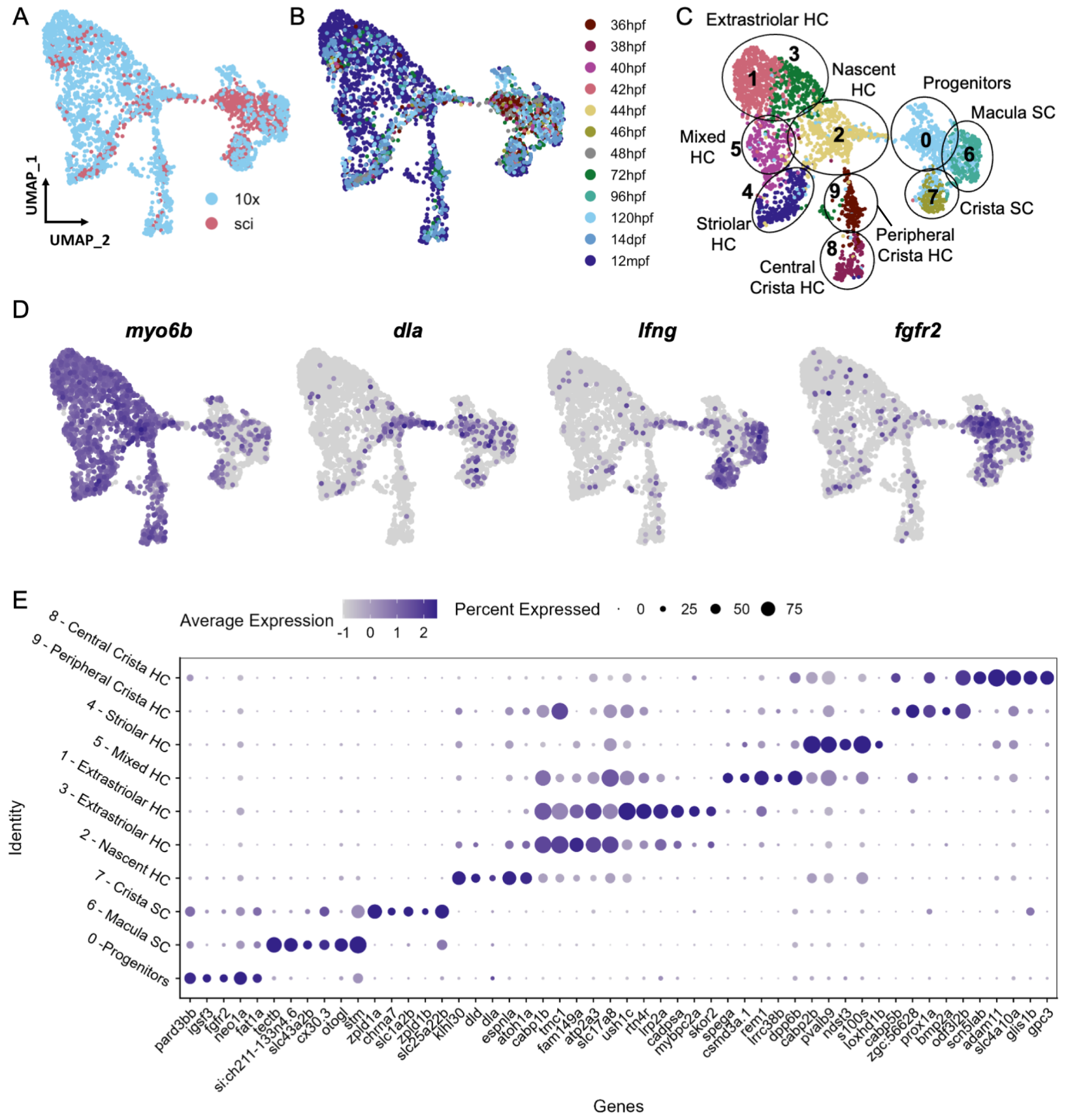
A
UMAP_1
UMAP_2
10x
sci
B
36hpf
38hpf
40hpf
42hpf
44hpf
46hpf
48hpf
72hpf
96hpf
120hpf
14dpf
12mpf
C
Extrastriolar HC
Nascent HC
Progenitors
Macula SC
Mixed HC
Striolar HC
Crista SC
Peripheral Crista HC
Central Crista HC
D
myo6b
dla
lfng
fgfr2
E
Average Expression
Percent Expressed
8 - Central Crista HC
9 - Peripheral Crista HC
4 - Striolar HC
5 - Mixed HC
1 - Extrastriolar HC
3 - Extrastriolar HC
2 - Nascent HC
7 - Crista SC
6 - Macula SC
0 -Progenitors
Identity
Genes

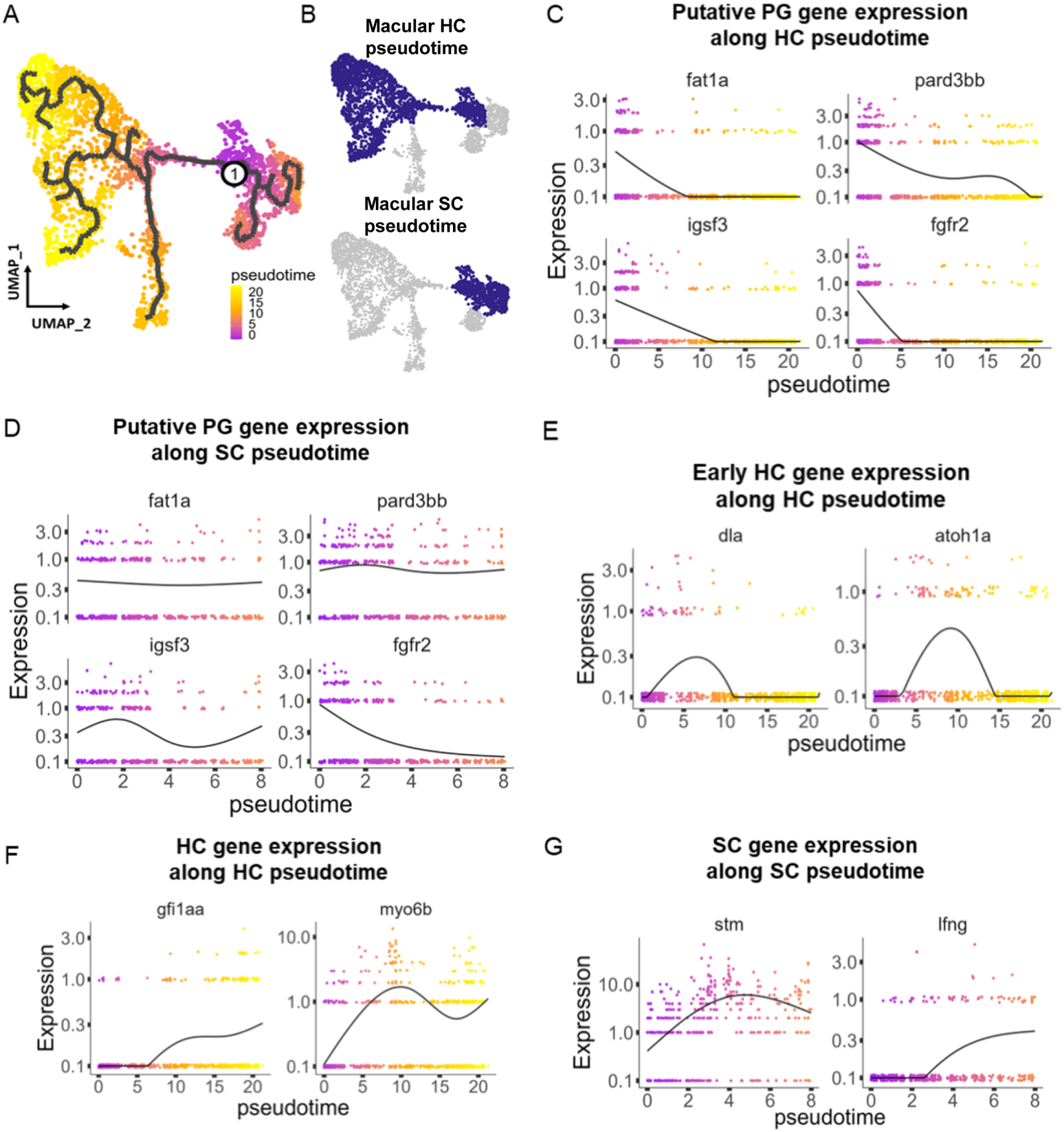
A
UMAP_1
UMAP_2
1
pseudotime
20
15
10
5
0
B
Macular HC pseudotime
Macular SC pseudotime
C
Putative PG gene expression along HC pseudotime
fat1a
pard3bb
igsf3
fgfr2
Expression
pseudotime
D
Putative PG gene expression along SC pseudotime
fat1a
pard3bb
igsf3
fgfr2
Expression
pseudotime
E
Early HC gene expression along HC pseudotime
dla
atoh1a
Expression
pseudotime
F
HC gene expression along HC pseudotime
gfi1aa
myo6b
Expression
pseudotime
G
SC gene expression along SC pseudotime
stm
lfng
Expression
pseudotime

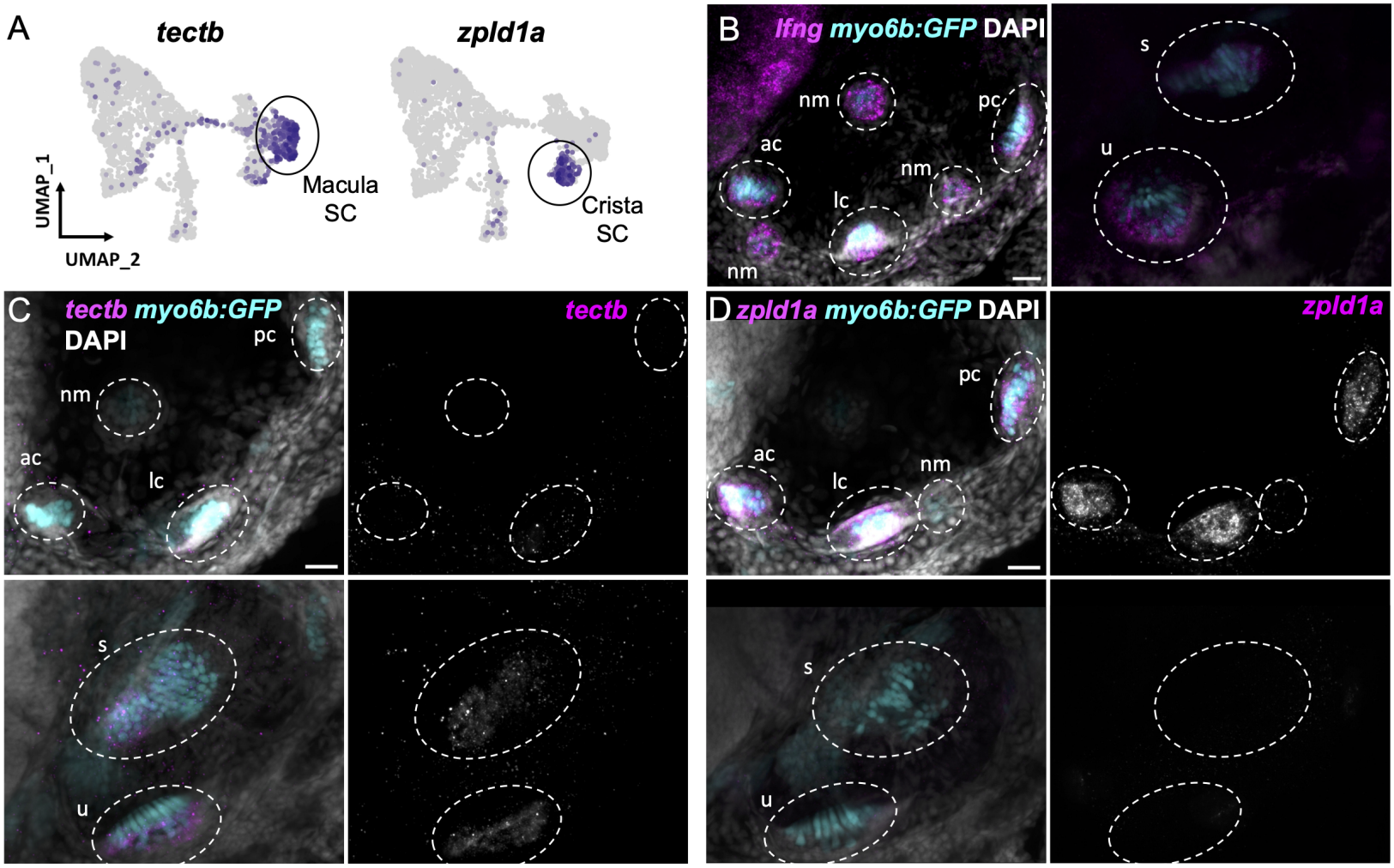
A
tectb
zpld1a
UMAP_1
UMAP_2
Macula SC
Crista SC
B
lfng myo6b:GFP DAPI
nm
pc
ac
nm
lc
nm
s
u
C
tectb myo6b:GFP
DAPI
pc
nm
ac
lc
tectb
s
u
D
zpld1a myo6b:GFP DAPI
pc
ac
lc
nm
zpld1a
s
u

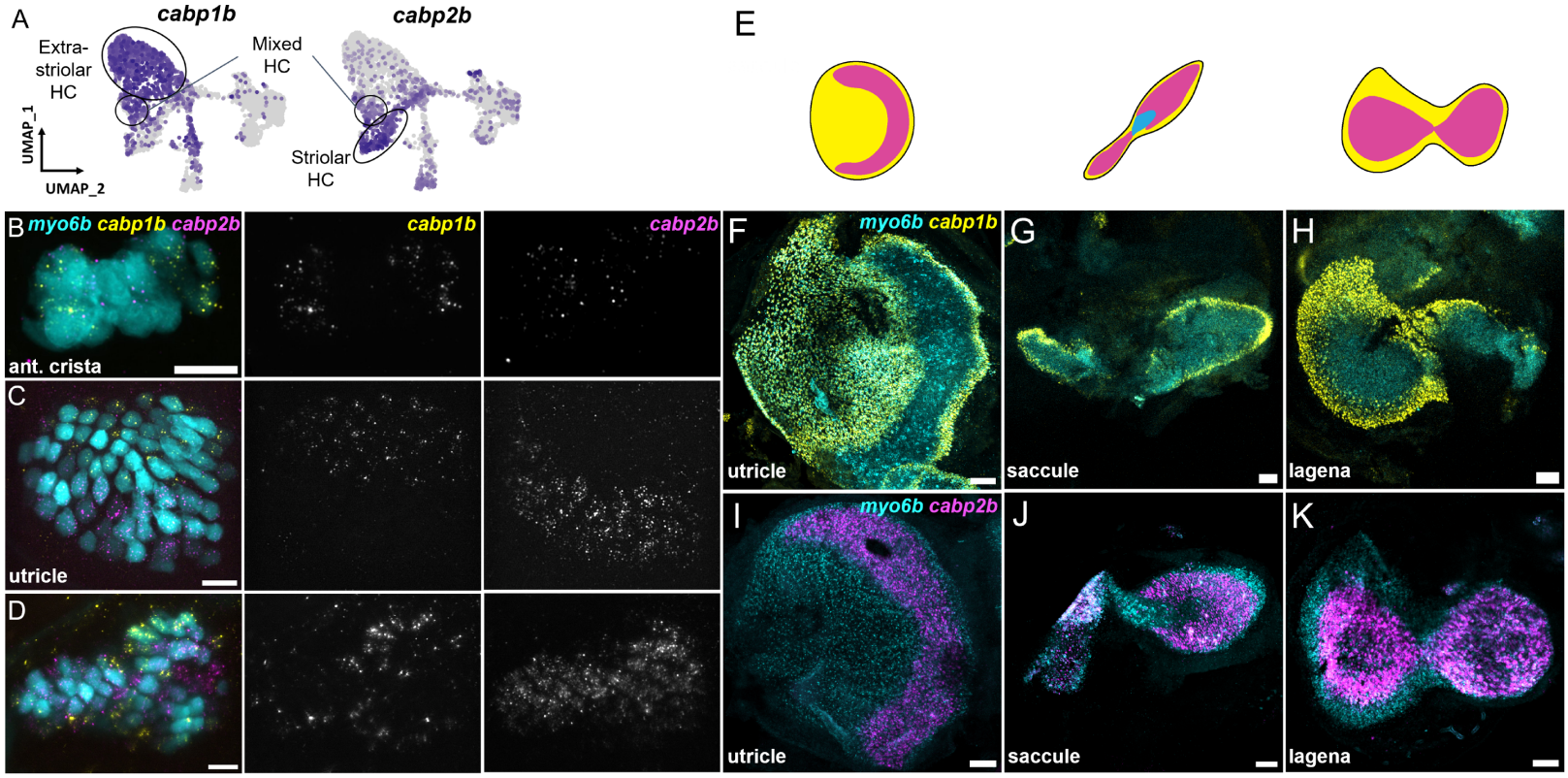
A
cabp1b
cabp2b
Extra-striolar HC
Mixed HC
Striolar HC
UMAP_1
UMAP_2
E
B myo6b cabp1b cabp2b
cabp1b
cabp2b
ant. crista
C
utricle
D
F myo6b cabp1b
utricle
G
saccule
H
lagena
I myo6b cabp2b
utricle
J
saccule
K
lagena

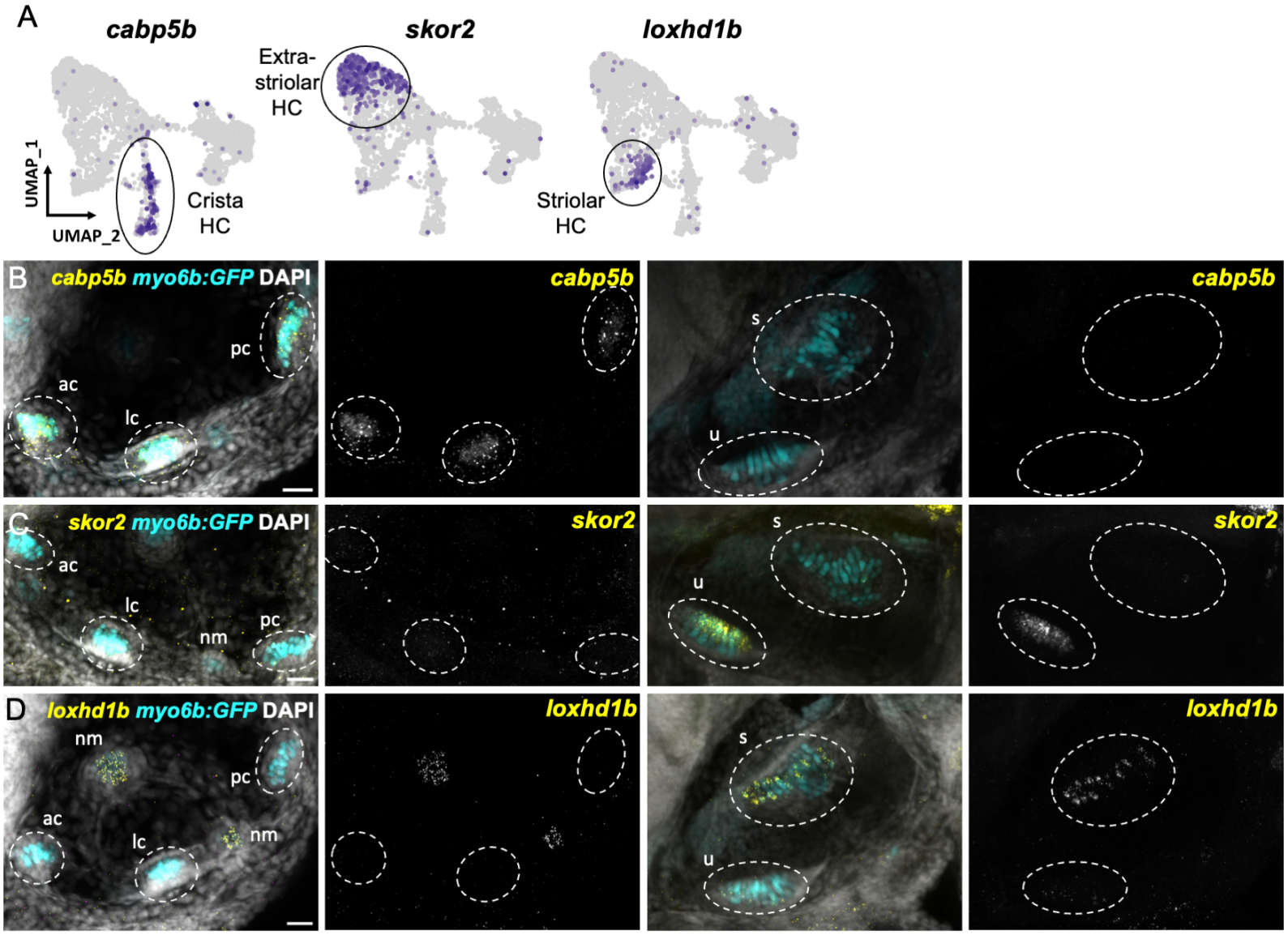
A
cabp5b
skor2
loxhd1b
Extra-striolar HC
Crista HC
Striolar HC
UMAP_1
UMAP_2
B
cabp5b myo6b:GFP DAPI
cabp5b
cabp5b
ac
lc
pc
s
u
C
skor2 myo6b:GFP DAPI
skor2
skor2
ac
lc
nm
pc
s
u
D
loxhd1b myo6b:GFP DAPI
loxhd1b
loxhd1b
nm
pc
ac
lc
nm
s
u

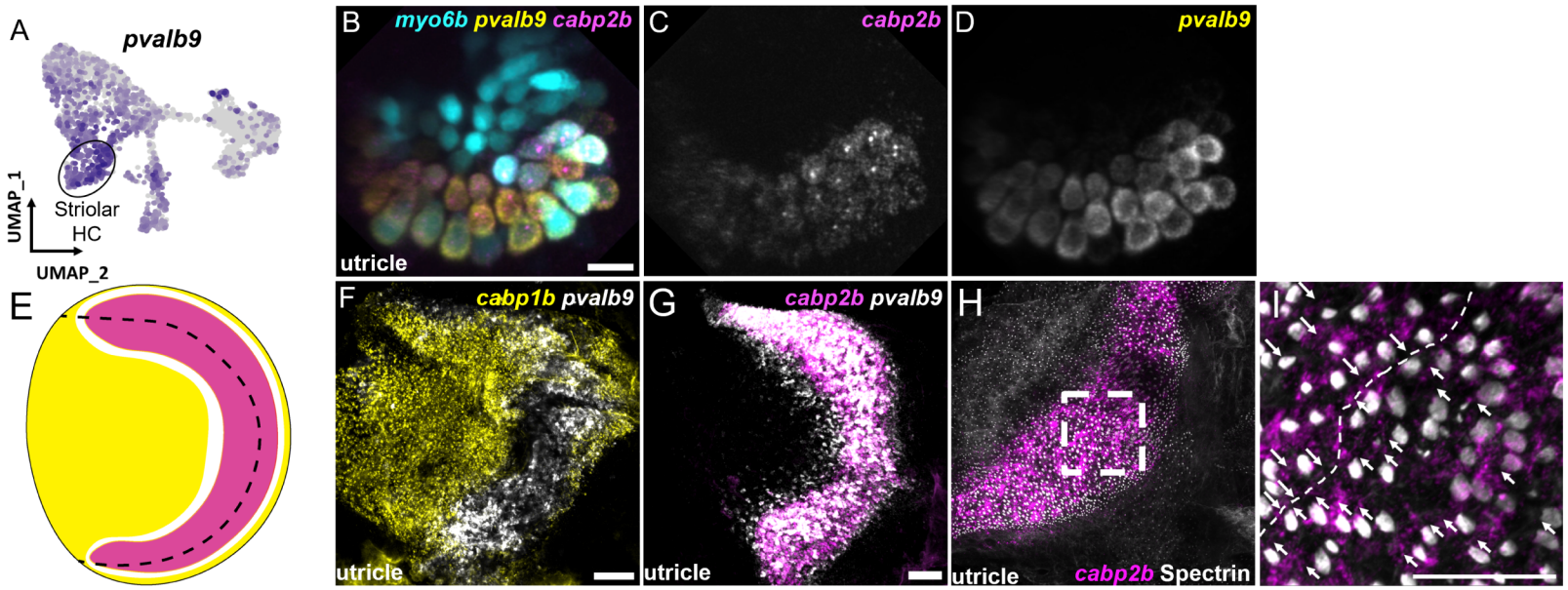
A
pvalb9
Striolar
HC
UMAP_1
UMAP_2
B
myo6b pvalb9 cabp2b
utricle
C
cabp2b
D
pvalb9
E
F
cabp1b pvalb9
utricle
G
cabp2b pvalb9
utricle
H
utricle
cabp2b Spectrin
I

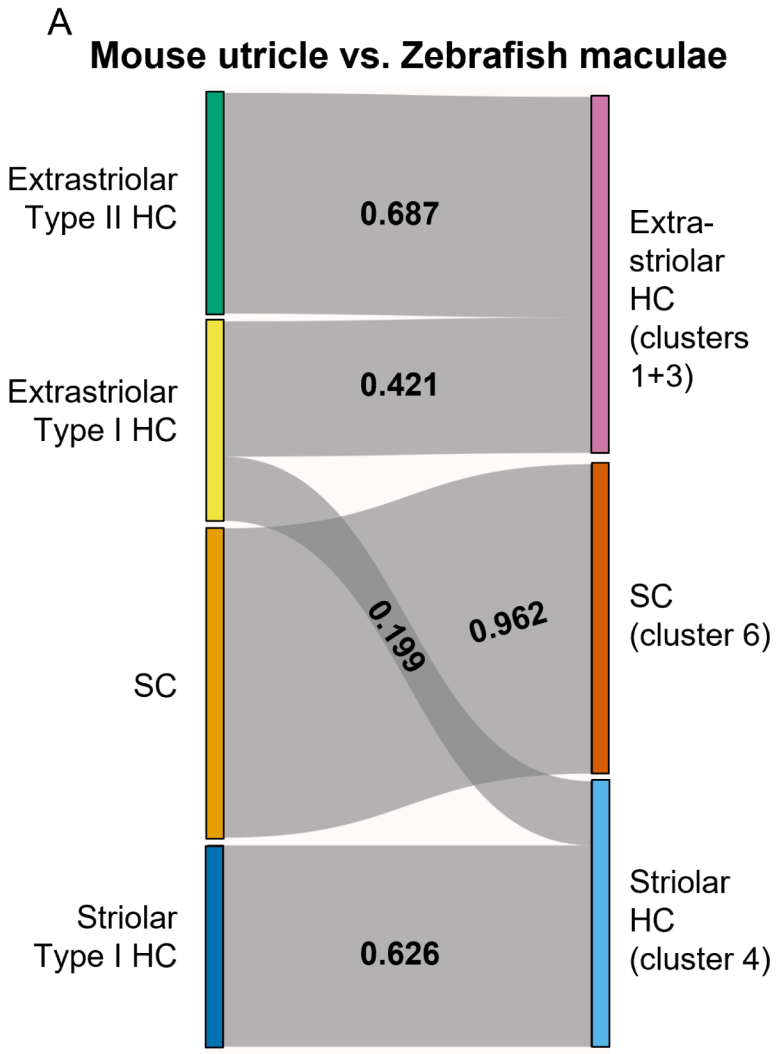
A
Mouse utricle vs. Zebrafish maculae
Extrastriolar Type II HC
Extrastriolar Type I HC
SC
Striolar Type I HC
0.687
0.421
0.199
0.962
0.626
Extra-striolar HC (clusters 1+3)
SC (cluster 6)
Striolar HC (cluster 4)

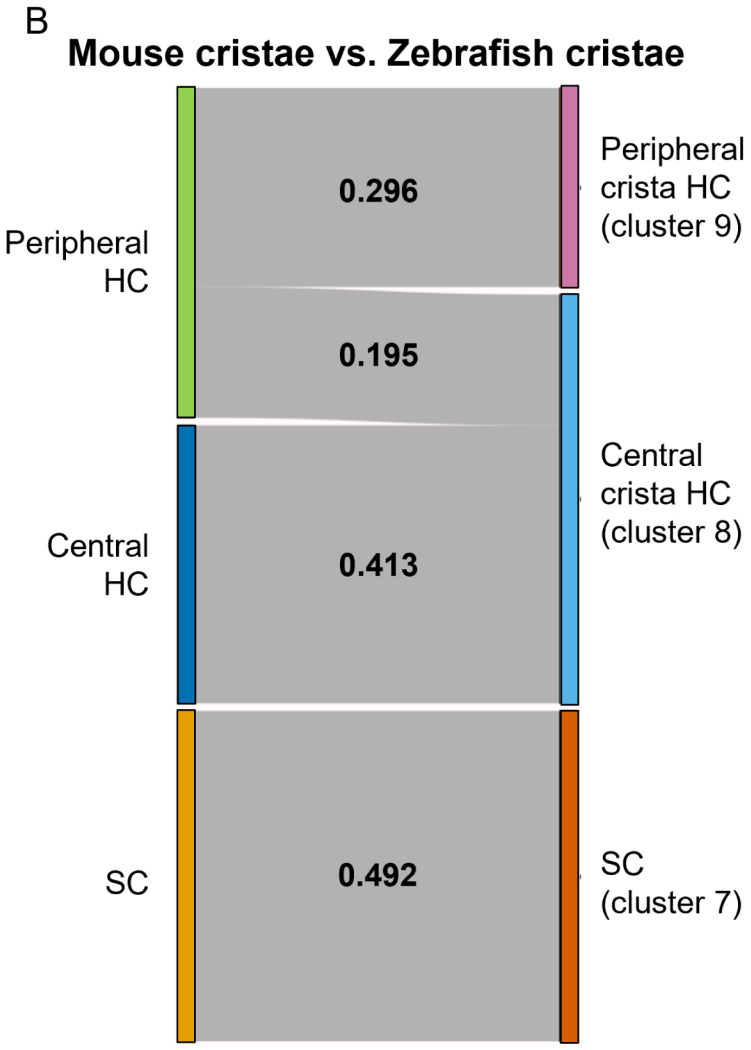
B
Mouse cristae vs. Zebrafish cristae
Peripheral HC
Central HC
SC
0.296
0.195
0.413
0.492
Peripheral crista HC (cluster 9)
Central crista HC (cluster 8)
SC (cluster 7)

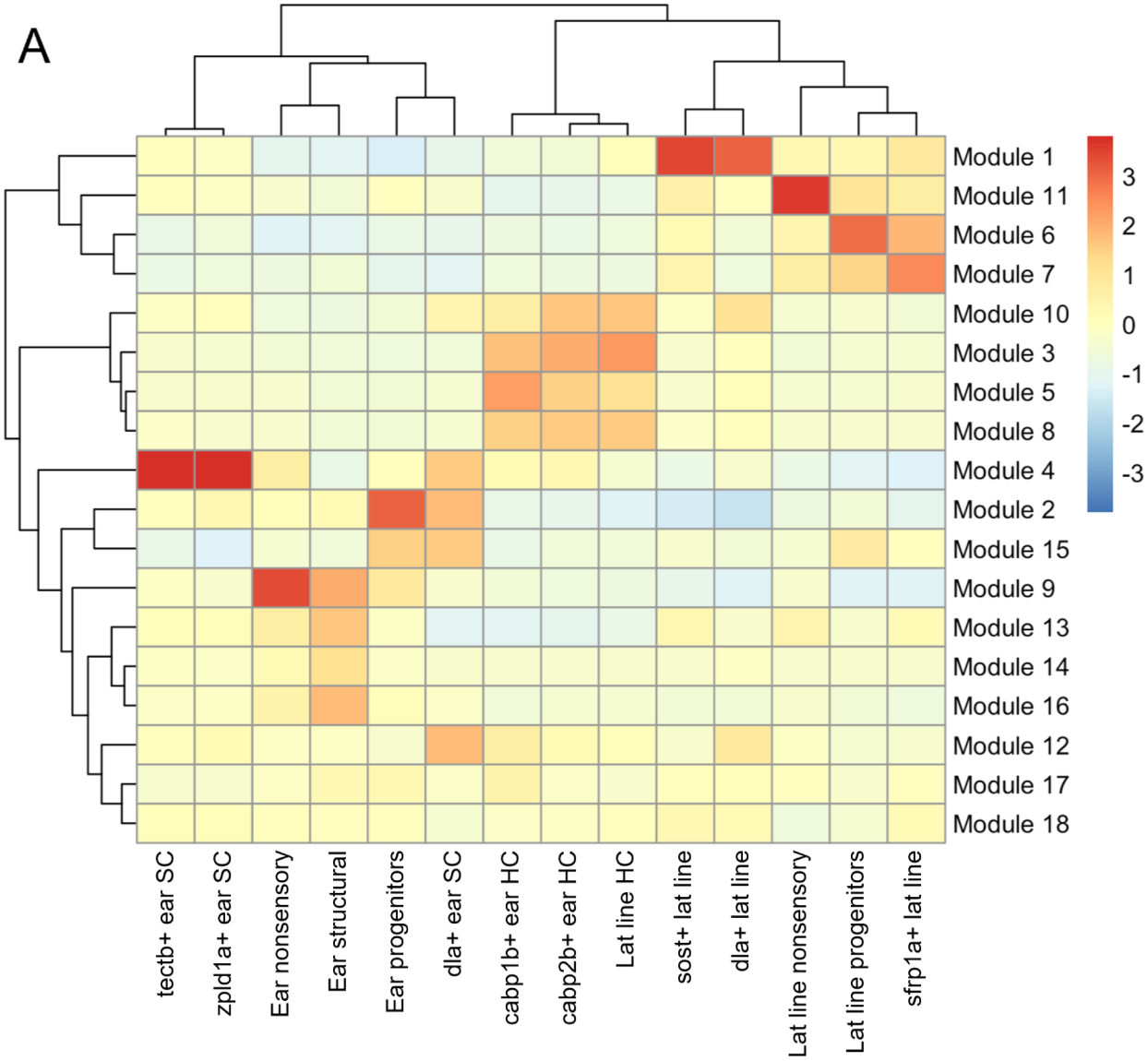
A
Module 1
Module 11
Module 6
Module 7
Module 10
Module 3
Module 5
Module 8
Module 4
Module 2
Module 15
Module 9
Module 13
Module 14
Module 16
Module 12
Module 17
Module 18
3
2
1
0
-1
-2
-3
tectb+ ear SC
zpld1a+ ear SC
Ear nonsensory
Ear structural
Ear progenitors
dla+ ear SC
cabp1b+ ear HC
cabp2b+ ear HC
Lat line HC
sost+ lat line
dla+ lat line
Lat line nonsensory
Lat line progenitors
sfrp1a+ lat line

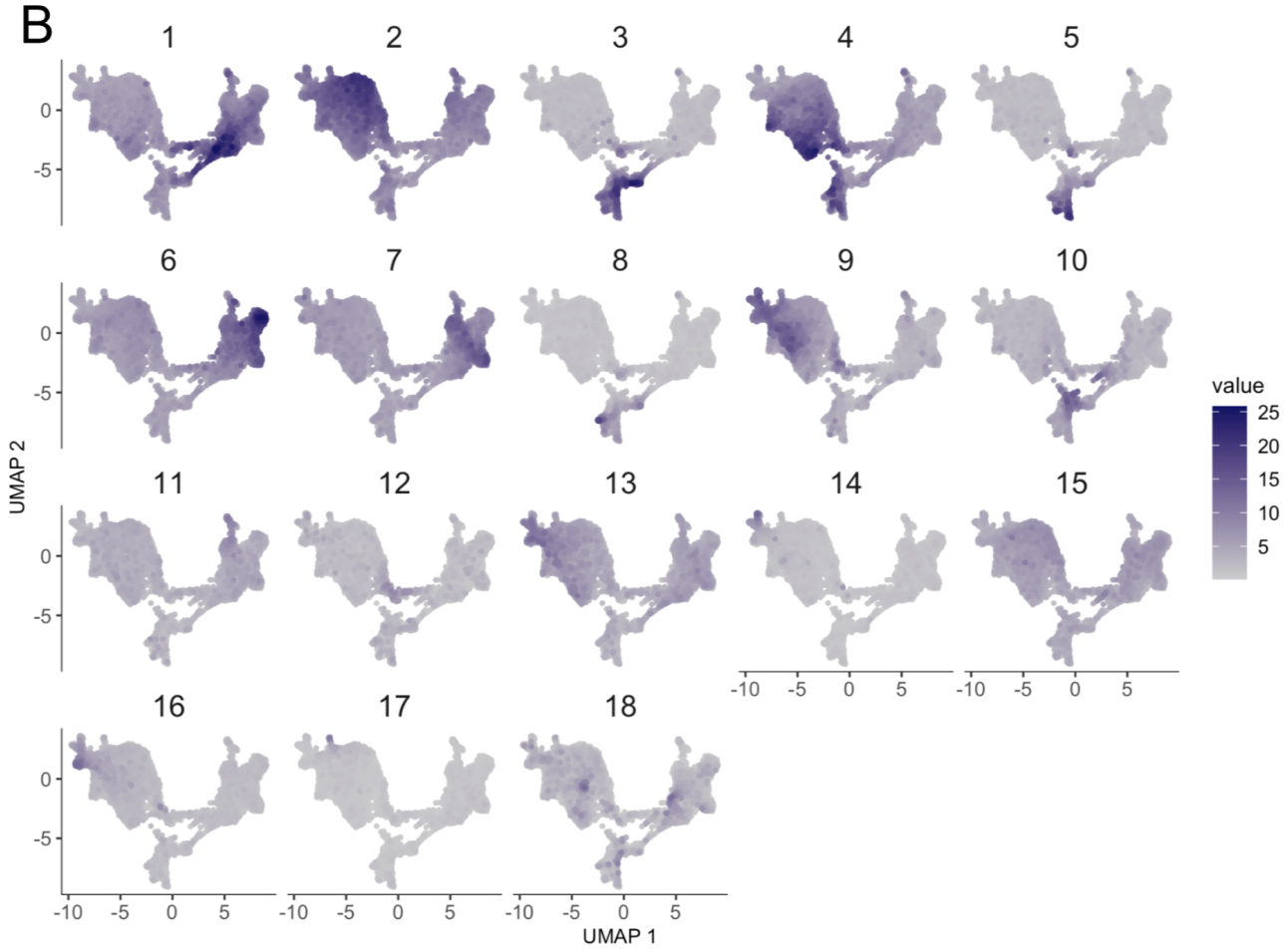
B
1
2
3
4
5
6
7
8
9
10
11
12
13
14
15
16
17
18
UMAP 2
UMAP 1
value
25
20
15
10
5

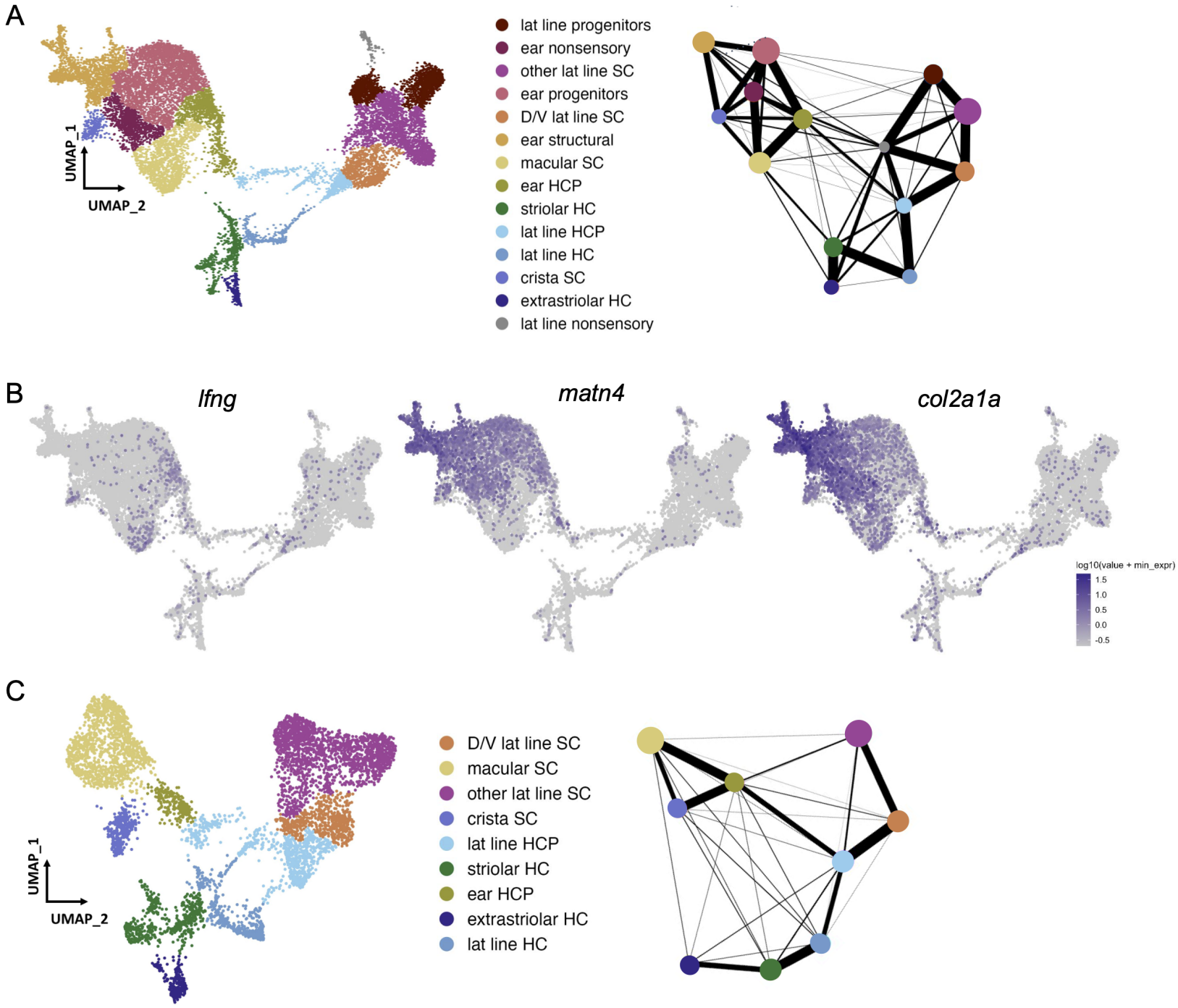
A
UMAP_1
UMAP_2
lat line progenitors
ear nonsensory
other lat line SC
ear progenitors
D/V lat line SC
ear structural
macular SC
ear HCP
striolar HC
lat line HCP
lat line HC
crista SC
extrastriolar HC
lat line nonsensory
B
lfng
matn4
col2a1a
log10(value + min_expr)
1.5
1.0
0.5
0.0
-0.5
C
UMAP_1
UMAP_2
D/V lat line SC
macular SC
other lat line SC
crista SC
lat line HCP
striolar HC
ear HCP
extrastriolar HC
lat line HC

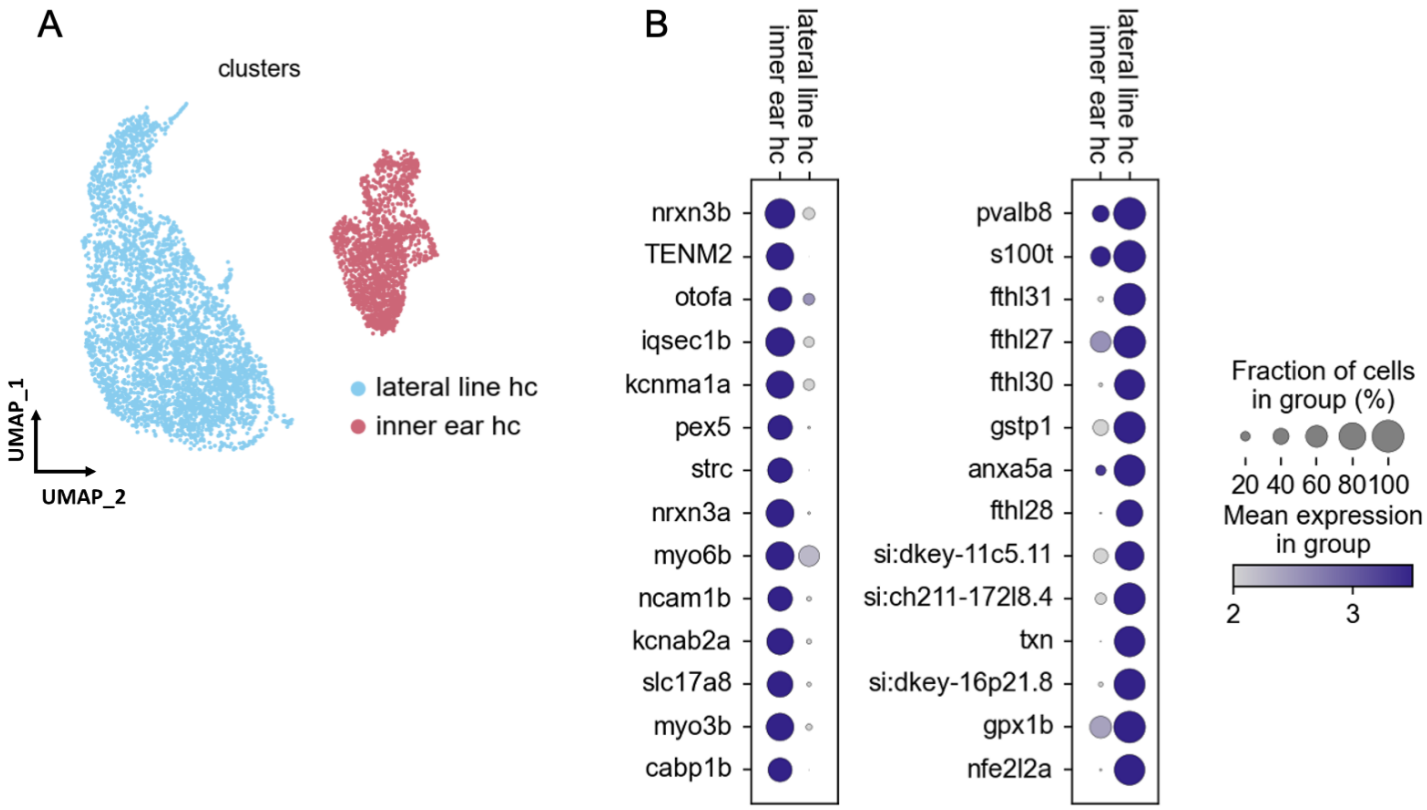
A
clusters
lateral line hc
inner ear hc
UMAP_1
UMAP_2
B
lateral line hc
inner ear hc
nrxn3b
TENM2
otofa
iqsec1b
kcnma1a
pex5
strc
nrxn3a
myo6b
ncam1b
kcnab2a
slc17a8
myo3b
cabp1b
pvalb8
s100t
fthl31
fthl27
fthl30
gstp1
anxa5a
fthl28
si:dkey-11c5.11
si:ch211-172l8.4
txn
si:dkey-16p21.8
gpx1b
nfe2l2a
Fraction of cells in group (%)
20 40 60 80 100
Mean expression in group
2
3

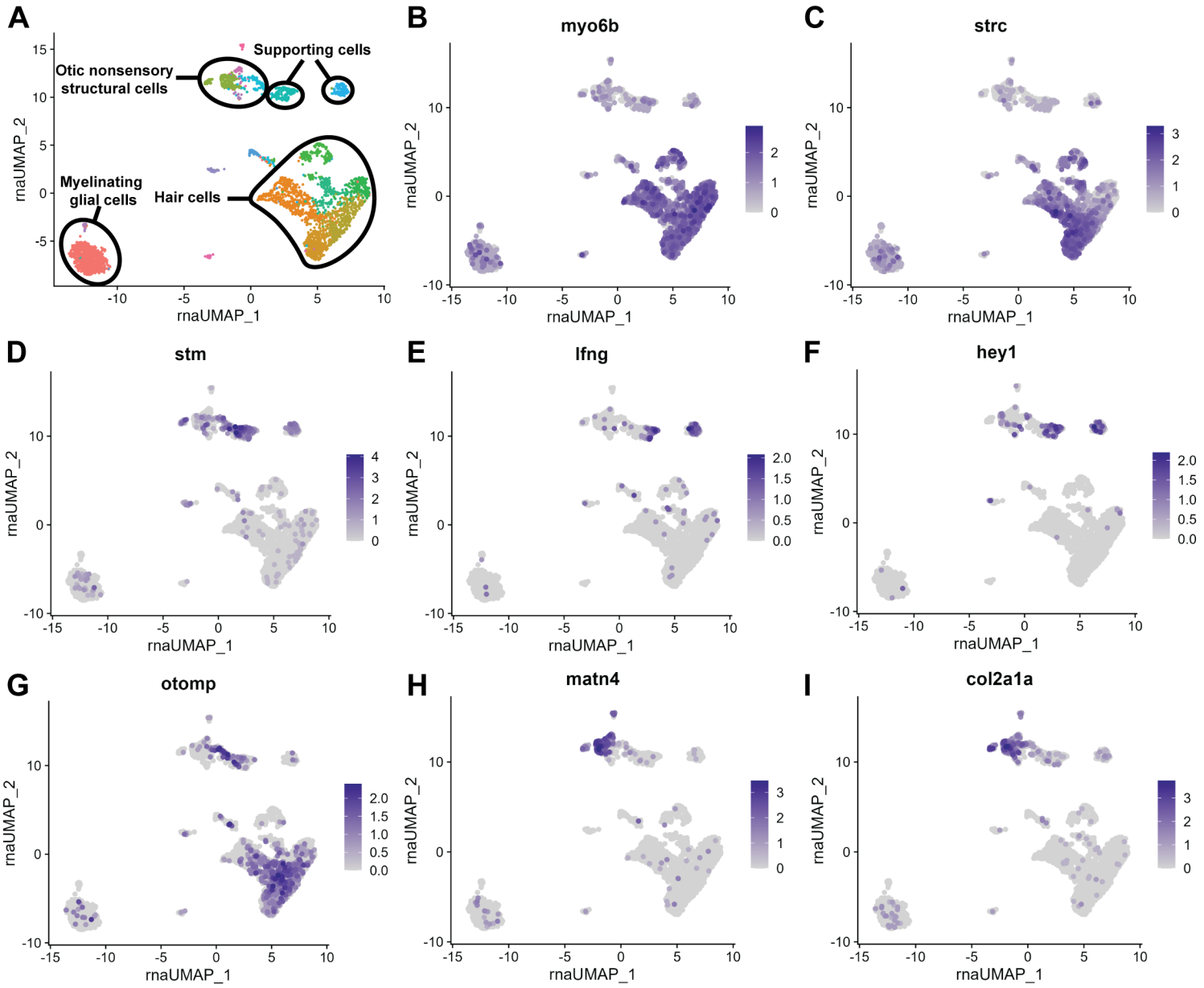
A
Supporting cells
Otic nonsensory structural cells
Myelinating glial cells
Hair cells
rnaUMAP_1
rnaUMAP_2
B
myo6b
C
strc
D
stm
E
lfng
F
hey1
G
otomp
H
matn4
I
col2a1a

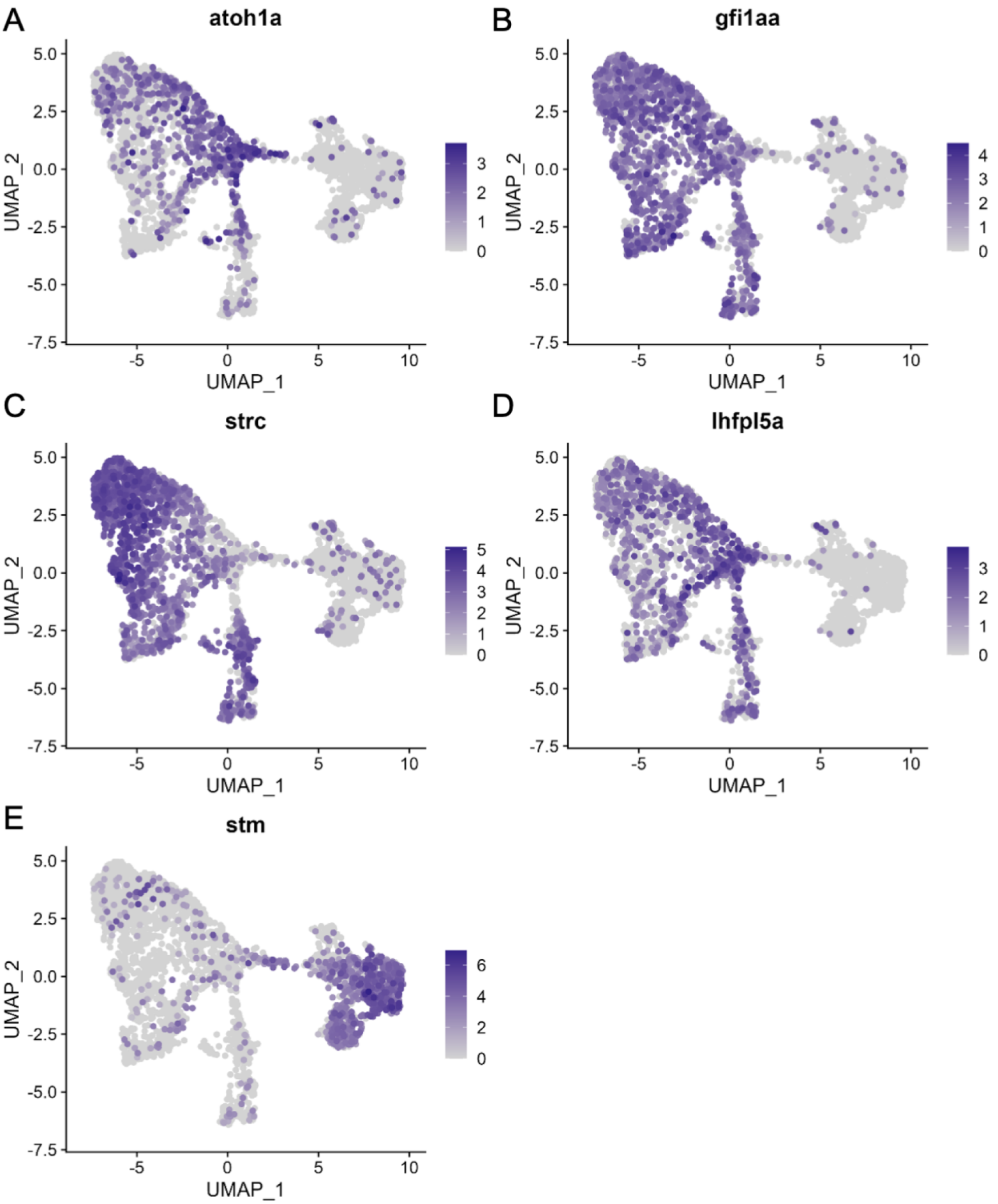
A
atoh1a
B
gfi1aa
C
strc
D
lhfpl5a
E
stm
UMAP_1
UMAP_2
5.0
2.5
0.0
-2.5
-5.0
-7.5
-5
0
5
10

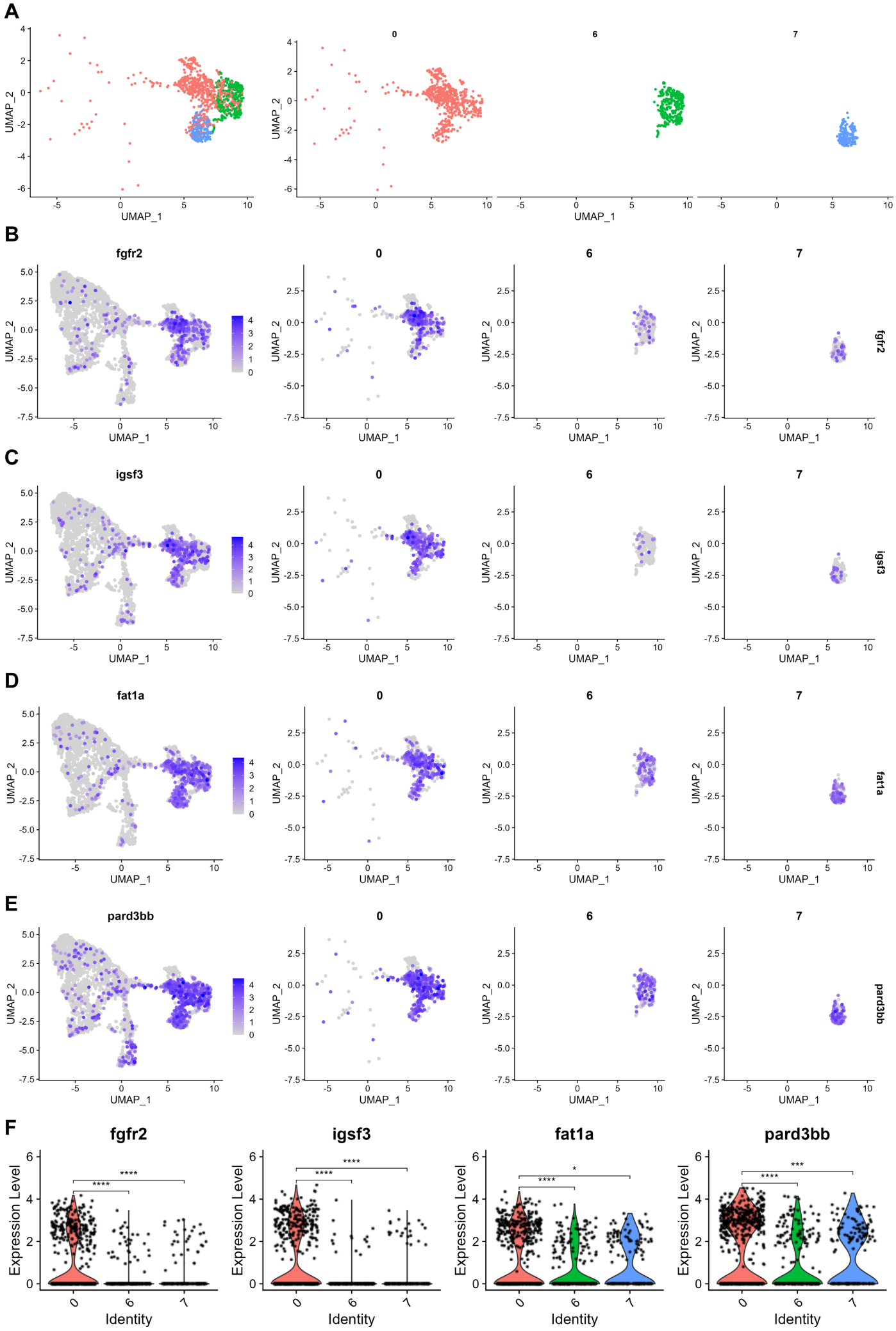
A
0
6
7
UMAP_1
UMAP_2
B
fgfr2
C
igsf3
D
fat1a
E
pard3bb
F
Expression Level
Identity
****
*
***

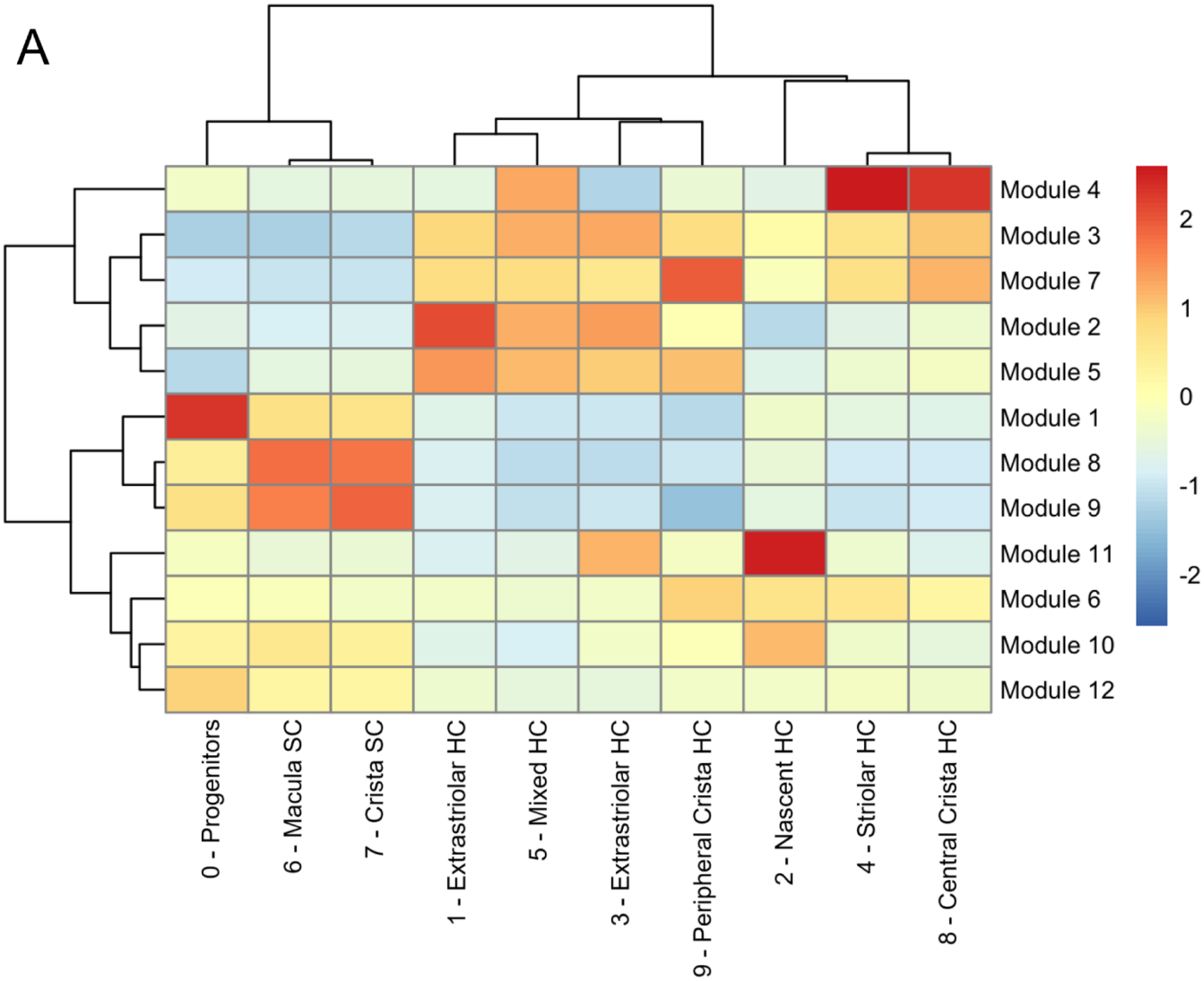
A
Module 4
Module 3
Module 7
Module 2
Module 5
Module 1
Module 8
Module 9
Module 11
Module 6
Module 10
Module 12
2
1
0
-1
-2
0 - Progenitors
6 - Macula SC
7 - Crista SC
1 - Extrastriolar HC
5 - Mixed HC
3 - Extrastriolar HC
9 - Peripheral Crista HC
2 - Nascent HC
4 - Striolar HC
8 - Central Crista HC

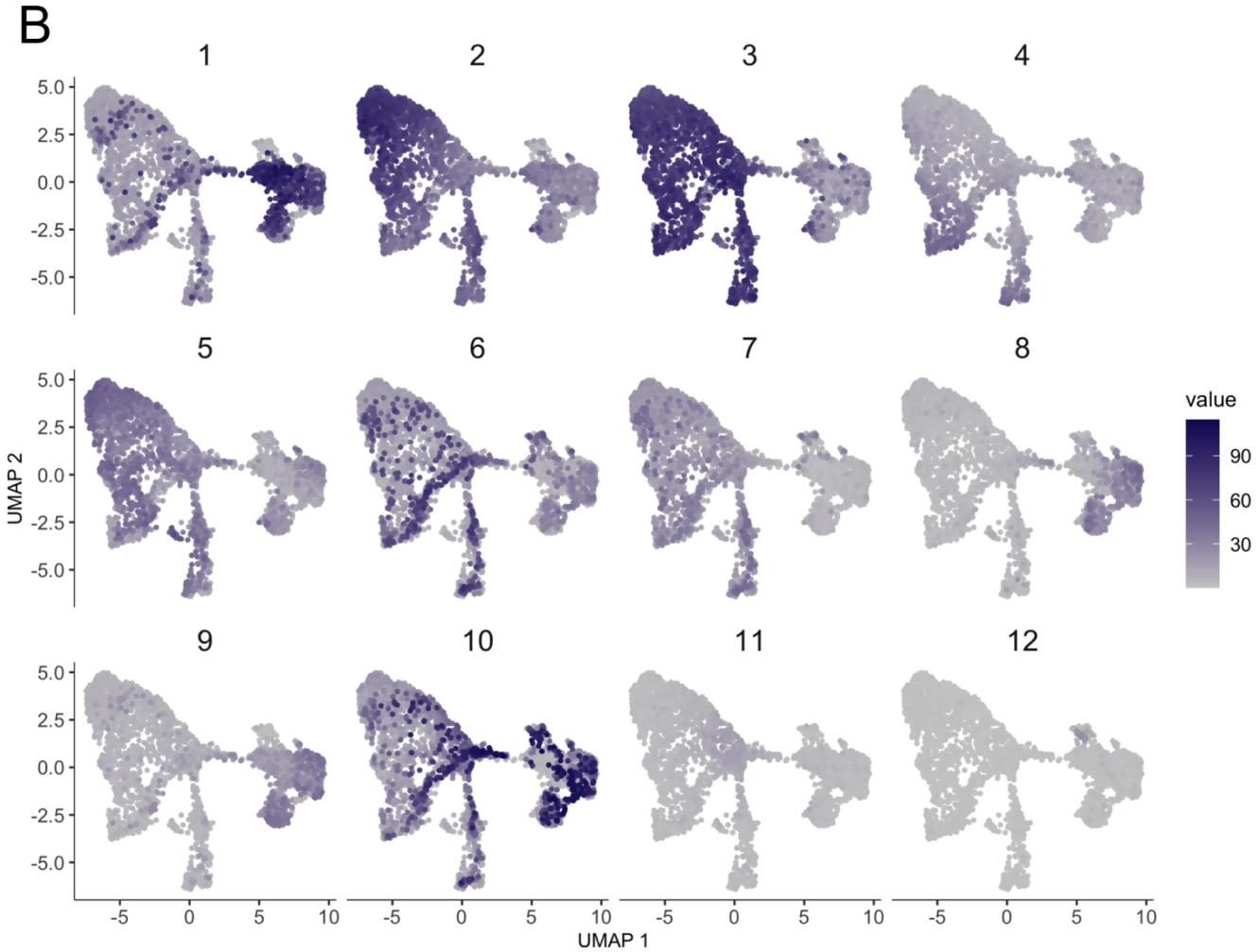
B
1
2
3
4
5
6
7
8
9
10
11
12
5.0
2.5
0.0
-2.5
-5.0
UMAP 2
-5
0
5
10
UMAP 1
value
90
60
30

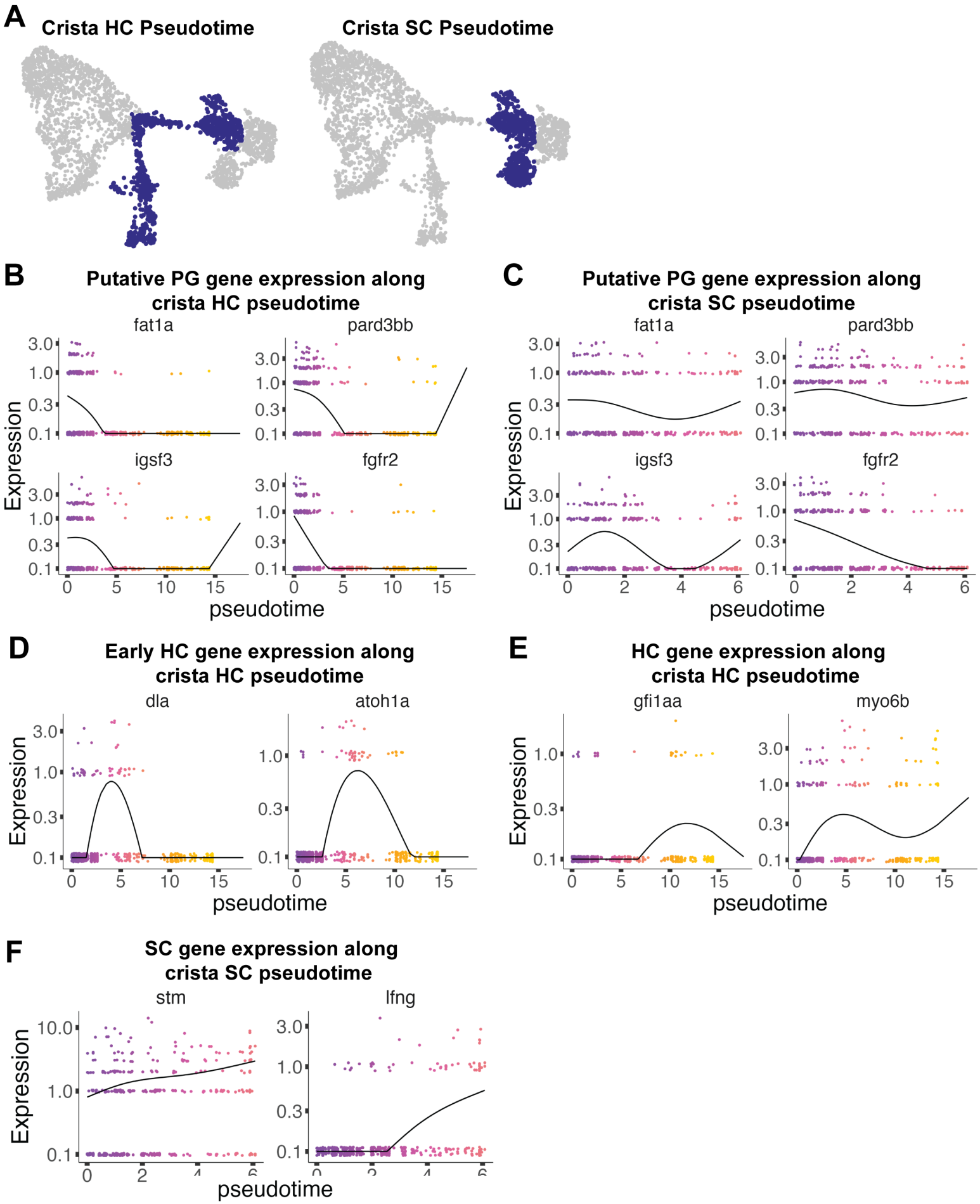
A
Crista HC Pseudotime
Crista SC Pseudotime
B
Putative PG gene expression along crista HC pseudotime
fat1a
pard3bb
igsf3
fgfr2
Expression
pseudotime
C
Putative PG gene expression along crista SC pseudotime
fat1a
pard3bb
igsf3
fgfr2
Expression
pseudotime
D
Early HC gene expression along crista HC pseudotime
dla
atoh1a
Expression
pseudotime
E
HC gene expression along crista HC pseudotime
gfi1aa
myo6b
Expression
pseudotime
F
SC gene expression along crista SC pseudotime
stm
lfng
Expression
pseudotime

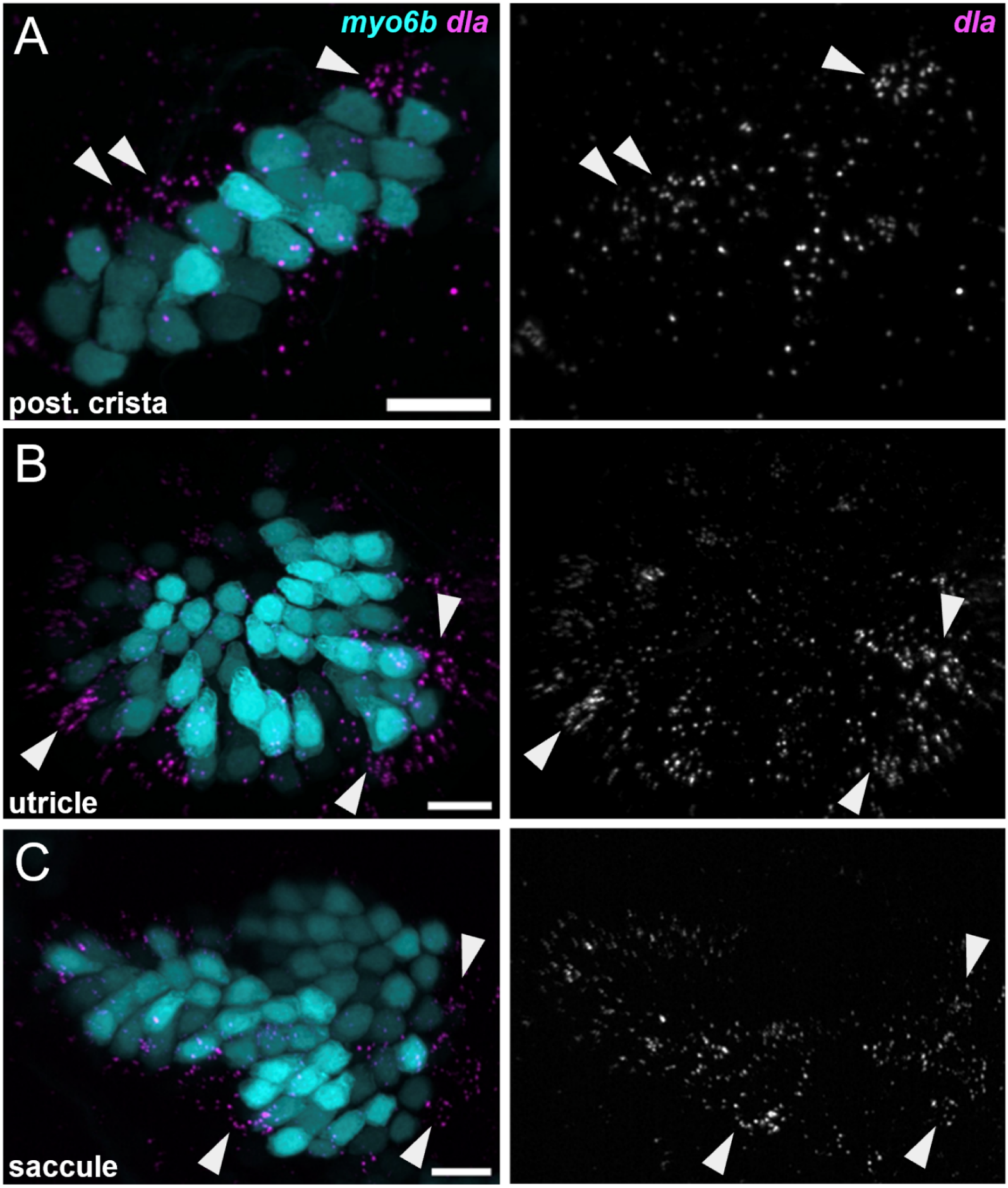
A
myo6b dla
dla
post. crista
B
utricle
C
saccule

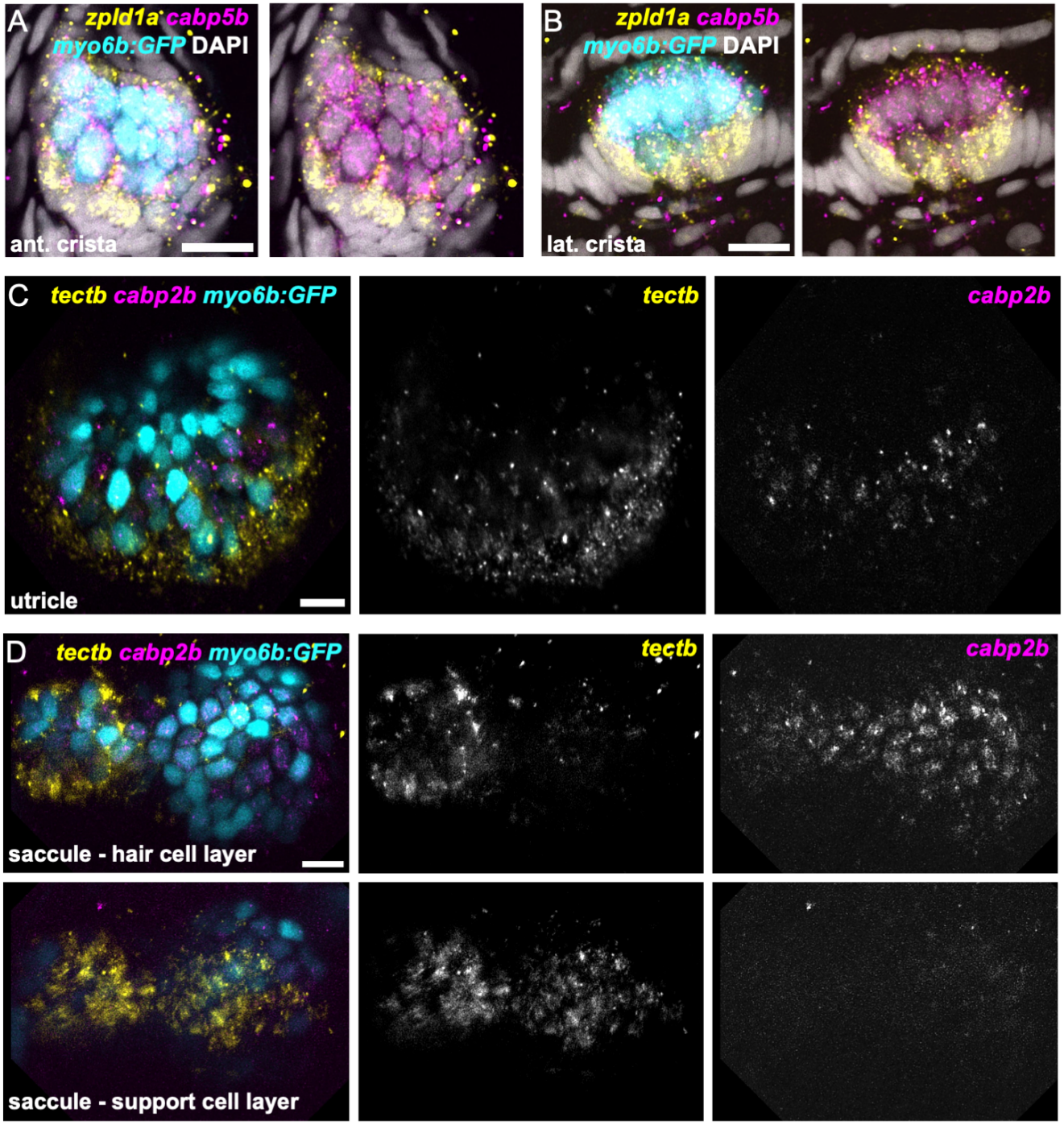
A
zpld1a cabp5b
myo6b:GFP DAPI
ant. crista
B
zpld1a cabp5b
myo6b:GFP DAPI
lat. crista
C
tectb cabp2b myo6b:GFP
utricle
tectb
cabp2b
D
tectb cabp2b myo6b:GFP
saccule - hair cell layer
tectb
cabp2b
saccule - support cell layer

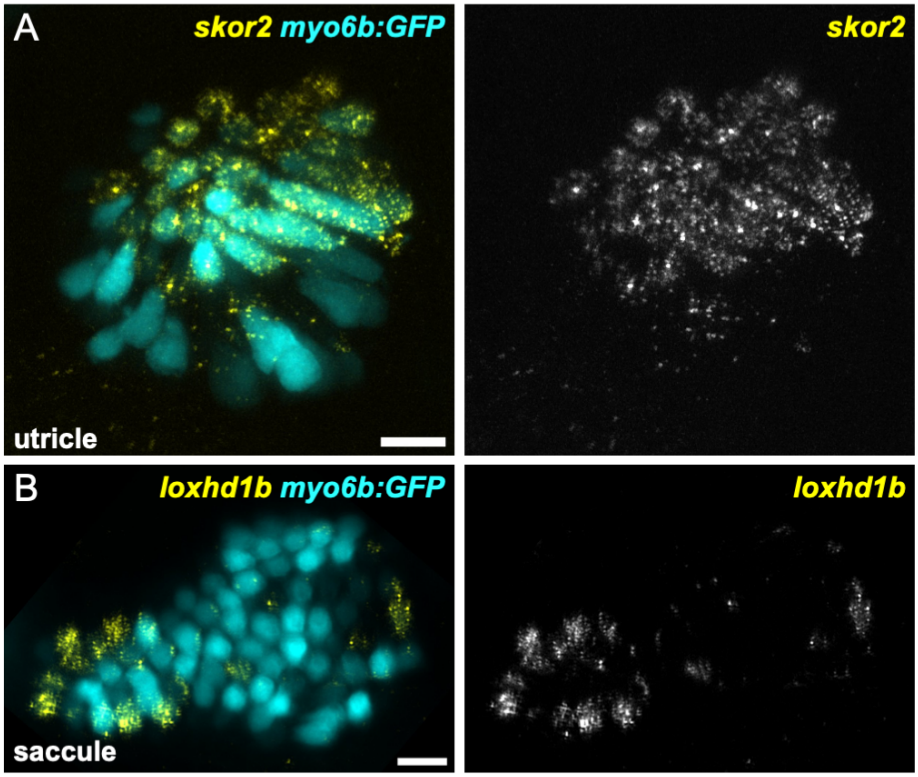
A
skor2 myo6b:GFP
skor2
utricle
B
loxhd1b myo6b:GFP
loxhd1b
saccule

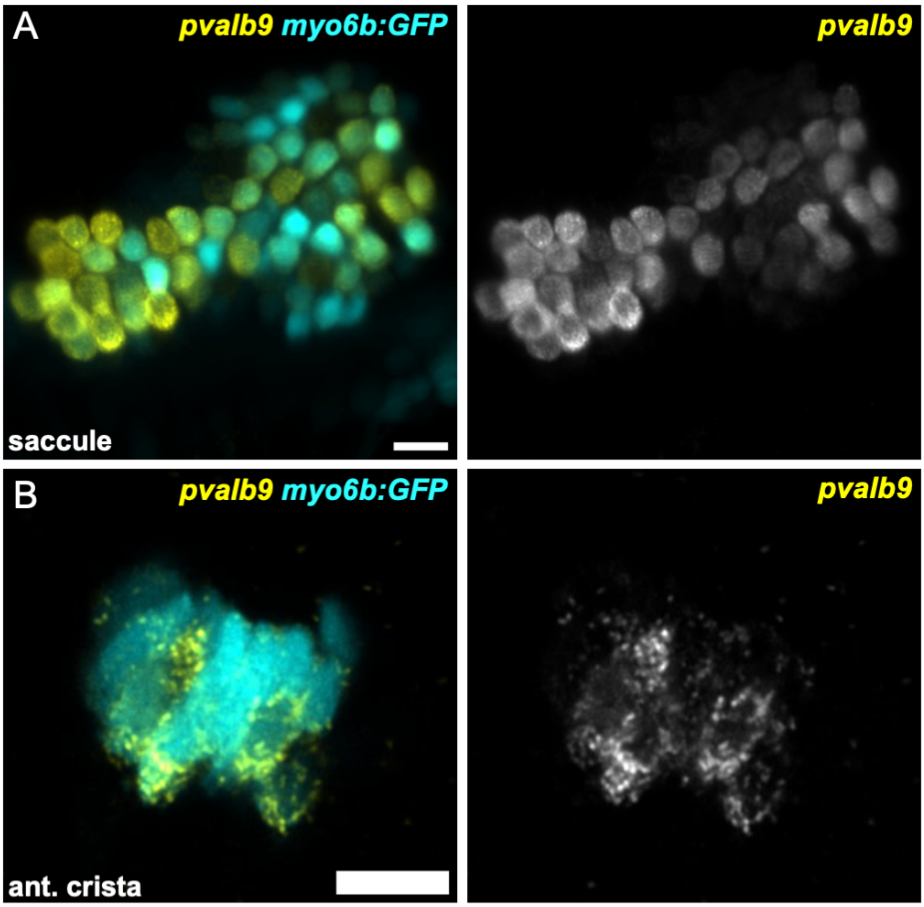
A
pvalb9 myo6b:GFP
pvalb9
saccule
B
pvalb9 myo6b:GFP
pvalb9
ant. crista

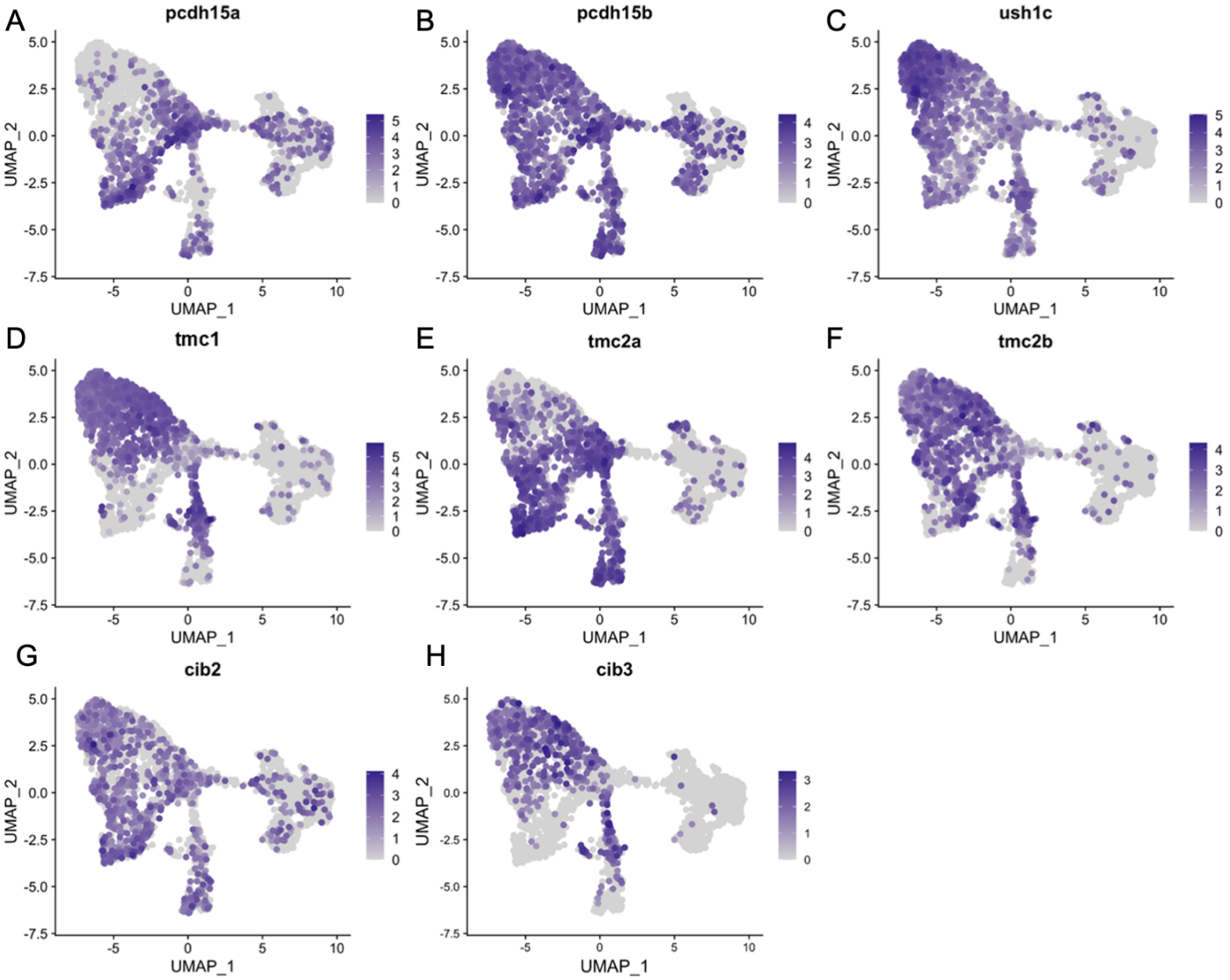
A
pcdh15a
B
pcdh15b
C
ush1c
D
tmc1
E
tmc2a
F
tmc2b
G
cib2
H
cib3
UMAP_1
UMAP_2

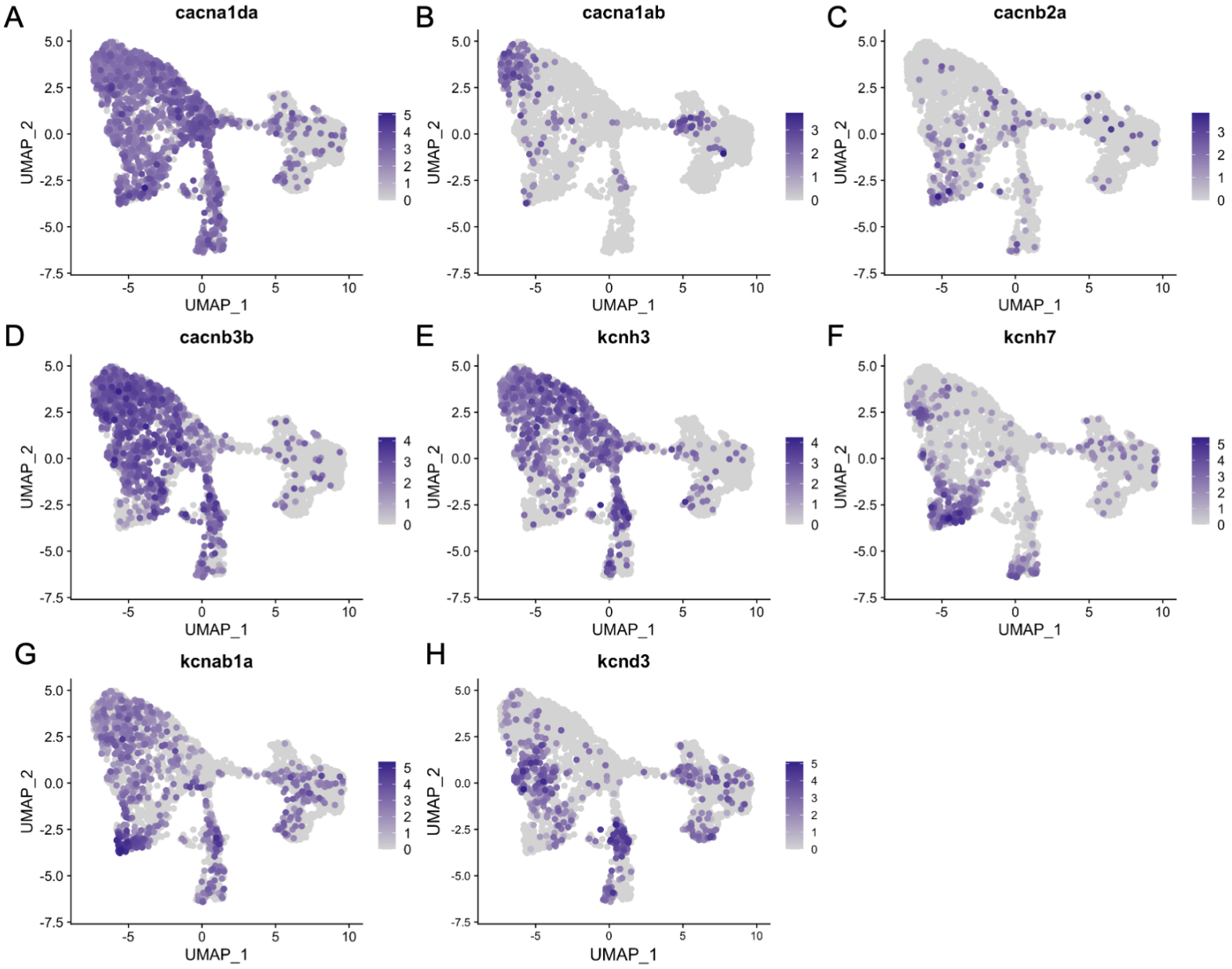
A
cacna1da
B
cacna1ab
C
cacnb2a
D
cacnb3b
E
kcnh3
F
kcnh7
G
kcnab1a
H
kcnd3
UMAP_1
UMAP_2

A

Mouse utricle vs.
Zebrafish maculae (12 mpf) &
lateral line (5 dpf)

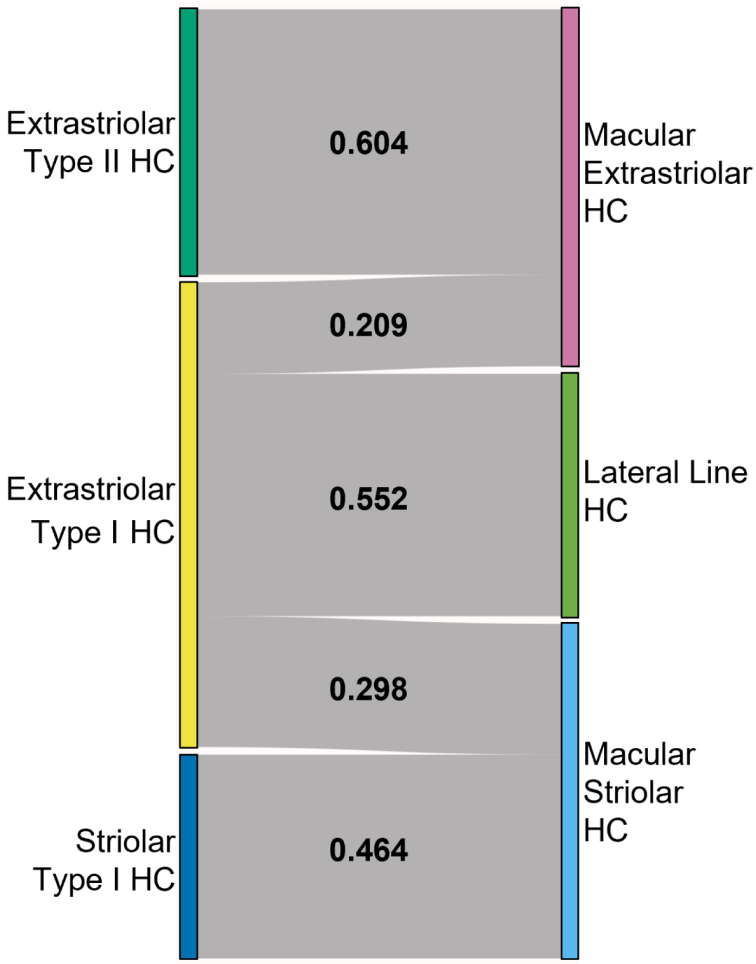

B

Mouse utricle vs.
Zebrafish maculae (3-5 dpf) &
lateral line (5 dpf)